

EFFICIENT AND LONG-TIME ACCURATE SECOND-ORDER DECOUPLED METHOD FOR THE BLOOD SOLUTE DYNAMICS MODEL

SABAH ATROUT, MD. ABDULLAH AL MAHBUB*, CHENYANG LI, AND HAIBIAO
ZHENG

Abstract. In this paper, we study the blood solute dynamics model to understand the relationship between the widespread pathologies of the vascular system, the specific features of the blood flow in a diseased district, and the effect of the flow pattern on the transfer processes of solute within arterial lumen and wall. The proposed finite element algorithm is based on the second-order backward differentiation formula and the explicit treatment of the coupling terms, which allow us to solve the decoupled Navier-Stokes equations, advection-diffusion equation, and pure diffusion equation at each time step. We derive the unconditional and long-time stability in the sense that the solution remains uniformly bounded in time, leading to uniform time error estimation. The long-time accurate behavior is one of the most desirable physical processes for the development of cardiovascular diseases that occurs over long-time scale. To validate the proposed method and demonstrate the exclusive features of the blood solute dynamical model, we perform four numerical experiments. Moreover, the impact of the development of atherosclerosis lesion and abdominal aortic aneurysm are studied by illustrating the complicated flow characteristics, streamlines, pressure contours, solute concentration, wall shear stress, and long-time accuracy on the several geometrical setups for the physiological interests.

Key words. Blood solute dynamics, second-order method, partitioned algorithm, unconditional stability, long-time stability.

1. Introduction

Over the past few decades, atherosclerosis and aneurysm considered as the most prevalent kind of cardiovascular diseases, have been studied extensively to identify the causes, genesis and the risk factors to achieve some methodologies for improving the human health by developing new prophylactic, diagnostic and therapeutic procedures [1, 3, 5, 4, 2, 6, 7, 8, 9]. Atherosclerosis is the hardening of large arteries due to the penetration and the development of the fatty plaque within the arterial wall, which leads to a gradual narrowing of the arteries. On the other hand, abdominal aortic aneurysms (AAAs) occur in the abdominal aortic artery where the artery has a balloon-shaped expansion; hence, the increase in the lumen diameter reaches up to 50 % of its standard diameter [2, 10, 11, 12, 13, 14]. Thus, the study of such cardiovascular diseases (atherosclerosis and aneurysm) involves the contribution of mass transport across the permeable endothelial layer and fluid dynamics of blood. On the other hand, in [10, 15], authors identified that hypertension is one of the main reason which enhanced the inner arterial wall due to the significant effects on the macromolecule distribution. Moreover, the dependence of shear stress on the solute transport from blood to the stenosis artery wall has been discussed in [11, 18, 16, 17].

Based on the arterial anatomy and the high dependence of the development of lesions on the transport procedure within the arteries, scientists have been set up

Received by the editors on May 1, 2024 and, accepted on June 26, 2025.

2000 *Mathematics Subject Classification.* 76D05, 76Z05, 76R50, 76M10, 65M60.

*Corresponding author.

some partial differential equation models and numerical tools to study the blood flow. In [16, 17, 19], the authors introduced the *wall-free* model to describe the dynamic of the macromolecules (Low-Density-Lipoprotein (LDL), albumin, oxygen, etc.) from the lumen to the arterial wall through the endothelial layer, which is considered as the common interface. The *wall-free* model is based on the coupling of the Navier-Stokes equations to describe the blood motion in the vascular tissue, the solute concentration in the lumen is modeled by the advection-diffusion equation, while the solute dynamics inside the wall is considered as a given quantity. On the other hand, a more sophisticated and realistic blood solute dynamics model is proposed in [20, 21, 22, 23] by considering the *fluid-wall* phenomena. In the *fluid-wall* model the solute dynamics into the vascular wall is taken into account and modeled by the pure diffusion equation by neglecting the convective field due to the small variety of blood velocity in the wall. Furthermore, the conservation of solute concentration and the exchange of flux of solute through the permeable membrane from lumen to the arterial wall are governed by two coupling conditions [22, 23]. In nature, the blood vessel is elastic, deform due to the cardiovascular system, while certain studies assumed the arterial wall as a rigid structure [19, 24].

It is worthwhile noting that many numerical methods have been developed to decouple the original problem for the accurate and efficient resolution of the multi-domain, and multiphysics problems [25, 26, 29, 27, 28, 33, 30, 31, 32]. The long-time feature is essential for the realization of the development of cardiovascular diseases, thus the long-time accuracy of the algorithm is highly desirable. Jiang investigated a second-order ensemble method based on a blended backward differentiation time-stepping algorithm for the time-dependent Navier-Stokes equations in [34]. The unconditional long-time stability for a particular velocity-vorticity discretization of the 2D Navier-Stokes equations studied in [35]. Hou et al. derived the second-order convergence of a projection scheme for the incompressible Navier-Stokes equations in [36]. Besides, the second-order schemes have been considered to decouple the system of Navier/Stokes-Darcy equations extensively. In [37], Layton et al. proposed uncoupled Crank-Nicolson Leapfrog (*CNLF*) and *BD2-AB2* schemes and derived the stability of the system. Chen et al. [38] proved the unconditional and uniform stability of two second-order *BDF2* and *AMB2* schemes, which imply the uniform control of the error. In [39], a third-order scheme has been studied, while in [40], the authors presented a second-order decouple scheme and uncouple the velocity and pressure by artificial compression method. A second-order partitioned method with different subdomain time steps for the evolutionary Stokes-Darcy system presented in [41]. In [42], Heister et al. considered the decoupled, unconditionally stable, higher-order discretizations for MHD flow simulation. The long-time stability of the extrapolated *BDF2* time-stepping methods for the Navier-Stokes equations and related multiphysics problems have been studied in [43]. Ravindran [44], proposed the second-order *BDF2* partitioned time-stepping algorithm for solving the transient viscoelastic fluid flow. Moreover, some numerical methods for the blood solute dynamics model have been presented. In [47], the author proposed a robust modified characteristics variational multiscale (MCVMS) method, which is based on the combination of the characteristics temporal discretization to deal with the difficulty caused due to the nonlinear terms, and the projection-based variational multiscale (VMS) technique to stabilize the spurious oscillation caused by the lower diffusivity of the solute concentration. Also, an IMEX scheme and a data-passing scheme for the blood model were considered in [46].

In this paper, we propose and analyze an efficient and long-time accurate second-order backward differentiation partitioned time-stepping algorithm for a sophisticated blood solute dynamics model governed by the Navier-Stokes equations for the blood flow motion and the advection-diffusion equations for the solute transport in the lumen, and pure diffusion equation to describe the solute concentration in the arterial wall. To the best of our knowledge, this is the first approach to investigate the blood solute dynamical model with the second-order long-time accurate decoupled finite element method. Herein, we discretize the system in time via second-order backward differentiation formula *BDF2* and the explicit treatment of the interface terms. Hence this numerical method leads to solve each subproblem independently at an individual time step, which allow us to use legacy code. We analyze the unconditional and long-time stability of the proposed scheme over a long-time interval $0 \leq t^n < \infty$ in the sense that the solutions remain uniformly bounded in time, which lead us to derive uniform in time error estimate. The optimal error estimates over the long-time interval for the proposed scheme are derived. Long-time accuracy is the highly desirable feature because one would want to have reliable numerical results over a long-time scale. The validity of the proposed scheme for the blood solute dynamical model is illustrated by performing four numerical experiments.

The rest of the manuscript is organized as follow. In Section 2, we introduce the blood solute dynamics model. Some notations, mathematical preliminaries, and variational formulation are presented in Section 3. The second-order decouple backward differentiation scheme *BDF2*, unconditional and long-time stability are discussed in Section 4. In Section 5, we derive the error estimation for the fully discrete scheme. In Section 6, numerical tests are presented to illustrate the stability, accuracy, and efficiency of the numerical method. At last, in Section 7, we report some concluding remarks.

2. Blood solute dynamics model description

In this section, we consider a multiphysics model of solute dynamics in the blood lumen and the arterial wall [22, 23, 46, 47], see Figure 1. The domain Ω consists of two subdomains including the lumen Ω_f and arterial wall Ω_w in $\mathbb{R}^d, d = 2, 3$. The common interface between the lumen and the arterial wall is denoted by $\Gamma = \partial\Omega_f \cap \partial\Omega_w$, which can be considered a permeable membrane.

The time-dependent Navier-Stokes equations is used to describe the incompressible Newtonian fluid flow in the lumen

$$(1) \quad \frac{\partial \mathbf{u}}{\partial t} + (\mathbf{u} \cdot \nabla) \mathbf{u} - \nu \Delta \mathbf{u} + \nabla p = \mathbf{f} \quad \text{in } \Omega_f, \quad t > 0,$$

$$(2) \quad \nabla \cdot \mathbf{u} = 0 \quad \text{in } \Omega_f, \quad t > 0,$$

$$(3) \quad \mathbf{u} = \mathbf{b} \quad \text{on } \partial\Omega_f \setminus \Gamma, \quad \mathbf{u} = 0 \quad \text{on } \Gamma, \quad t > 0,$$

$$(4) \quad \mathbf{u} = \mathbf{u}_0 \quad \text{with } \nabla \cdot \mathbf{u}_0 = 0 \quad \text{on } \Omega_f, \quad t = 0,$$

here $\mathbf{u} : \Omega_f \times \mathbb{R}^+ \rightarrow \mathbb{R}^d$ is the fluid velocity, $p : \Omega_f \times \mathbb{R}^+ \rightarrow \mathbb{R}$ is the kinematic pressure, \mathbf{f} is the external force and ν is the kinematic viscosity. Moreover, \mathbf{b} and \mathbf{u}_0 are the given boundary (on $\partial\Omega_f \setminus \Gamma$) and initial data.

The solute concentration in the lumen is governed by the advection-diffusion equation

$$(5) \quad \frac{\partial C_f}{\partial t} - \nabla \cdot (\mu_f \nabla C_f) + \mathbf{u} \cdot \nabla C_f = f_f \quad \text{in } \Omega_f, \quad t > 0,$$

$$(6) \quad C_f = 0 \quad \text{on } \partial\Omega_f \setminus \Gamma, \quad t > 0,$$

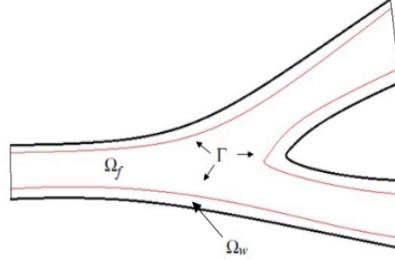


FIGURE 1. Geometrical description of the arterial lumen and the wall.

where $C_f : \Omega_f \times \mathbb{R}^+ \rightarrow \mathbb{R}$ is the concentration of the considered solute in the domain Ω_f , μ_f is the diffusivity tensor which is a function of the rate of deformation tensor \mathbf{d} , such that $\mathbf{d}_{ij} = \frac{1}{2}(\frac{\partial u_i}{\partial x_j} + \frac{\partial u_j}{\partial x_i})$, $i, j = 1, 2, \dots, d$ and f_f is the force term, which could be the effect of the chemical interaction between the solute and other molecules in the blood.

Because the velocity inside the wall domain is very low, the solute dynamics is modeled by the pure diffusion equation

$$(7) \quad \frac{\partial C_w}{\partial t} - \nabla \cdot (\mu_w \nabla C_w) = f_w \quad \text{in } \Omega_w, \quad t > 0,$$

$$(8) \quad C_w = 0 \quad \text{on } \partial\Omega_w \setminus \Gamma, \quad t > 0,$$

such that, $C_w : \Omega_w \times \mathbb{R}^+ \rightarrow \mathbb{R}$ denote the solute concentration in the arterial wall, μ_w is the diffusivity tensor and f_w is a source term in the wall.

We consider the matching conditions at the interface Γ [22, 23], such that

$$(9) \quad \mu_w \frac{\partial C_w}{\partial n_w} = -n_f \cdot (\mu_f \nabla C_f) \quad \text{on } \Gamma,$$

$$(10) \quad n_f \cdot (\mu_f \nabla C_f) + \zeta(C_f - C_w) = 0 \quad \text{on } \Gamma,$$

where n_f and n_w are the unit normal vectors to the lumen and arterial wall, respectively. The positive definite Lipschitz continuous function ζ denotes the permeability of the wall, which is a function of the shear stress $\sigma(\mathbf{u})$, $\zeta = |\sigma(\mathbf{u})|$, such that $\sigma(\mathbf{u}) = \tau \cdot T(\mathbf{u}) \cdot n_f$ and $T(\mathbf{u}) = 2\nu\mathbf{d}$, where τ is the tangential vector on the wall.

It is worthwhile noting that the first interface condition (9) guarantees the conservation of solute concentration in both domains Ω_f and Ω_w . On the other hand, the second coupling condition (10) indicates that the exchange of flux solute through the permeable membrane Γ is related to the difference of concentration in the lumen and the wall multiplied by the permeability ζ .

3. Notations and preliminaries

In this section, we define the following functional spaces and notations. The inner product in $L^2(\Omega)$ space and its induced norm is denoted by (\cdot, \cdot) and $\|\cdot\|$, respectively. Furthermore, the $L^\infty(\Omega)$ norm is denoted by $\|\cdot\|_\infty$ and H^s denotes the Hilbert space of functions and its distributional derivatives of order $0 \leq s$ in $L^2(\Omega)$. To set the variational formulation of solute dynamics in blood flow and

arterial walls, we define the following spaces [45].

$$\begin{aligned} V &:= H_0^1(\Omega_f)^d = \{\mathbf{v} \in H^1(\Omega_f)^d : \mathbf{v} = 0 \text{ on } \partial\Omega_f\}, \\ Q &:= L_0^2(\Omega_f) = \{q \in L^2(\Omega_f) : \int_{\Omega_f} q dx = 0\}, \\ X_f &:= H_{\partial\Omega_f \setminus \Gamma}^1(\Omega_f) = \{C_f \in H^1(\Omega_f) : C_f = 0 \text{ on } \partial\Omega_f \setminus \Gamma\}, \\ X_w &:= H_{\partial\Omega_w \setminus \Gamma}^1(\Omega_w) = \{C_w \in H^1(\Omega_w) : C_w = 0 \text{ on } \partial\Omega_w \setminus \Gamma\}. \end{aligned}$$

Define the product space

$$X = X_f \times X_w = \{(C_f, C_w); \forall C_f \in X_f, C_w \in X_w\},$$

which is equipped with the following norm

$$\|C_{fw}\|^2 = \|C_f\|^2 + \|C_w\|^2, \quad \forall C_{fw} \in X.$$

The variational formulation of the equation (1)–(10) is given as: find $\mathbf{u} \in L^2(0, T; V) \cap L^\infty(0, T; (L^2(\Omega_f))^d)$, $p \in L^2(0, T; Q)$, $C_f \in L^2(0, T; X_f)$ and $C_w \in L^2(0, T; X_w)$, $\forall t \in (0, T]$ and $\forall (\mathbf{v}, q, \phi_f, \phi_w) \in (V, Q, X_f, X_w)$, such that

$$(11) \quad \left(\frac{\partial \mathbf{u}}{\partial t}, \mathbf{v} \right) + \nu(\nabla \mathbf{u}, \nabla \mathbf{v}) + C^*(\mathbf{u}, \mathbf{u}, \mathbf{v}) - (\nabla \cdot \mathbf{v}, p) = (\mathbf{f}, \mathbf{v}),$$

$$(12) \quad (\nabla \cdot \mathbf{u}, q) = 0,$$

$$(13) \quad \left(\frac{\partial C_f}{\partial t}, \phi_f \right) + (\mu_f \nabla C_f, \nabla \phi_f) + b^*(\mathbf{u}, C_f, \phi_f) + (C_f - C_w, \phi_f)_\Gamma = (f_f, \phi_f),$$

$$(14) \quad \left(\frac{\partial C_w}{\partial t}, \phi_w \right) + (\mu_w \nabla C_w, \nabla \phi_w) + (C_w - C_f, \phi_w)_\Gamma = (f_w, \phi_w),$$

such that the skew-symmetric form of the trilinear terms can be written as [43]

$$(15) \quad C^*(\mathbf{u}, \mathbf{v}, \mathbf{w}) = \frac{1}{2}((\mathbf{u} \cdot \nabla) \mathbf{v}, \mathbf{w}) - \frac{1}{2}((\mathbf{u} \cdot \nabla) \mathbf{w}, \mathbf{v}) \quad \forall \mathbf{u}, \mathbf{v}, \mathbf{w} \in V,$$

$$(16) \quad b^*(\mathbf{u}, C_f, \phi_f) = \frac{1}{2}((\mathbf{u} \cdot \nabla) C_f, \phi_f) - \frac{1}{2}((\mathbf{u} \cdot \nabla) \phi_f, C_f) \quad \forall \mathbf{u} \in V; C_f, \phi_f \in X_f.$$

By adapting the results illustrated in [48], we introduce following lemma for the trilinear forms.

Lemma 1. [56] For all $\mathbf{u}, \mathbf{v}, \mathbf{w} \in V; C_f, \phi_f \in X_f$

$$\begin{aligned} C^*(\mathbf{u}, \mathbf{v}, \mathbf{w}) &= -C^*(\mathbf{u}, \mathbf{w}, \mathbf{v}), \\ b^*(\mathbf{u}, C_f, \phi_f) &= -b^*(\mathbf{u}, \phi_f, C_f), \\ |C^*(\mathbf{u}, \mathbf{v}, \mathbf{w})| &\leq \bar{c} \|\nabla \mathbf{u}\| \|\nabla \mathbf{v}\| \|\nabla \mathbf{w}\|, \\ |b^*(\mathbf{u}, C_f, \phi_f)| &\leq c \|\nabla \mathbf{u}\| \|\nabla C_f\| \|\nabla \phi_f\|. \end{aligned}$$

Next, we recall the following basic inequalities, [45, 49].

Trace inequality: If c_{trf} and c_{trw} are strictly positive constants depending on the domain Ω_f and Ω_w , respectively but independent of mesh size such that $\mathbf{v} \in V(\text{or } X_f)$ and $\phi \in X_w$ satisfies

$$\begin{aligned} \|\mathbf{v}\|_\Gamma &\leq c_{trf} \|\mathbf{v}\|^{\frac{1}{2}} \|\nabla \mathbf{v}\|^{\frac{1}{2}}, \quad \|\mathbf{v}\|_\Gamma \leq c_{trf} \|\nabla \mathbf{v}\|. \\ \|\phi\|_\Gamma &\leq c_{trw} \|\phi\|^{\frac{1}{2}} \|\nabla \phi\|^{\frac{1}{2}}, \quad \|\phi\|_\Gamma \leq c_{trw} \|\nabla \phi\|. \end{aligned}$$

Poincaré inequality: If c_{pf} and c_{pw} are strictly positive constants depending on the domain Ω_f and Ω_w , respectively but independent of mesh size such that for $\mathbf{v} \in V(\text{or } X_f)$ and $\phi \in X_w$ satisfies

$$\| \mathbf{v} \| \leq c_{pf} \| \nabla \mathbf{v} \|, \quad \| \phi \| \leq c_{pw} \| \nabla \phi \|.$$

Young's inequality: $\forall a, b, c, \epsilon \geq 0$, we have

$$a^{\frac{1}{2}} b^{\frac{1}{2}} c \leq \frac{\epsilon}{2} a^2 + \frac{b^2}{8\epsilon^3} + \frac{\epsilon}{2} c^2.$$

Standard inequality: If $d = \dim(\Omega_f)$ and $\mathbf{u} \in V$, we have

$$\| \nabla \cdot \mathbf{u} \| \leq \sqrt{d} \| \nabla \mathbf{u} \|.$$

We introduce a family of regular finite element triangulations $\{T_{fh}\}_{h>0}$ (resp. $\{T_{wh}\}_{h>0}$) of the domain Ω_f (resp. Ω_w), where the subscript h refer to the level of refinement of the triangulations. The simulation time T can be divided into N smaller time intervals with $[0, T] = \bigcup_{n=0}^{N-1} [t^n, t^{n+1}]$, where $t^n = n\Delta t$, $\Delta t = \frac{T}{N}$.

Denote $(V_h, Q_h, X_{fh}, X_{wh}) \subset (V, Q, X_f, X_w)$ the conforming finite element spaces which contain piecewise continuous polynomials of degree (k) and $(k-1)$ such that

$$\begin{aligned} V_h &:= \{ \mathbf{v}_h \in C(\Omega_f)^d, \mathbf{v}_h|_K \in P_k(K)^d, \forall K \in T_{fh} \}, \\ Q_h &:= \{ q_h \in C(\Omega_f), q_h|_K \in P_{k-1}(K), \forall K \in T_{fh} \}, \\ X_{fh} &:= \{ C_{fh} \in C(\Omega_f), C_{fh}|_K \in P_k(K), \forall K \in T_{fh} \}, \\ X_{wh} &:= \{ C_{wh} \in C(\Omega_w), C_{wh}|_K \in P_k(K), \forall K \in T_{wh} \}, \\ W_h &:= \{ \mathbf{v}_h \in V_h : (\nabla \cdot \mathbf{v}_h, q_h) = 0 \quad \forall q_h \in Q_h \}. \end{aligned}$$

The finite element spaces of the velocity and pressure (V_h, Q_h) are assumed to satisfy the discrete inf – sup condition

$$\inf_{q_h \in Q_h} \sup_{\mathbf{v}_h \in X_h} \frac{(q_h, \nabla \cdot \mathbf{v}_h)}{\| q_h \| \| \nabla \mathbf{v}_h \|} \geq \beta > 0,$$

such that β is independent of the mesh size h . The above finite element spaces satisfy the following approximation properties

$$\begin{aligned} (17) \quad & \inf_{\mathbf{v}_h \in V_h} \{ \| \mathbf{u} - \mathbf{v}_h \| + h \| \nabla(\mathbf{u} - \mathbf{v}_h) \| \\ & \leq ch^{k+1} \| \mathbf{u} \|_{k+1} \quad \forall \mathbf{u} \in H^{k+1}(\Omega_f)^d \cap V, \\ & \inf_{q_h \in Q_h} \| p - q_h \| \leq ch^k \| p \|_k, \quad \forall p \in H^k(\Omega_f)^d \cap Q \\ & \inf_{\phi_f \in X_{fh}} \{ \| C_f - \phi_{fh} \| + h \| \nabla(C_f - \phi_{fh}) \| \} \\ & \leq ch^{k+1} \| C_f \|_{k+1} \quad \forall C_f \in H^{k+1}(\Omega_f)^d \cap X_f, \\ & \inf_{\phi_w \in X_{wh}} \{ \| C_w - \phi_{wh} \| + h \| \nabla(C_w - \phi_{wh}) \| \} \\ & \leq ch^{k+1} \| C_w \|_{k+1} \quad \forall C_w \in H^{k+1}(\Omega_w)^d \cap X_w. \end{aligned}$$

4. Numerical scheme and its stability

In this section, we propose the second-order backward differentiation partitioned time-stepping scheme for the blood solute dynamics problem and the explicit treatment of the interface terms. Moreover, we prove the unconditional stability and long-time stability of the proposed algorithm.

4.1. The second-order backward differentiation partitioned time-stepping scheme (BDF2). **Algorithm.** Suppose that $\Delta t > 0$, for each $N = \frac{T}{\Delta t}$, given $(\mathbf{u}_h^{n-1}, C_{fh}^{n-1}, C_{wh}^{n-1}), (\mathbf{u}_h^n, C_{fh}^n, C_{wh}^n) \in V_h \times X_{fh} \times X_{wh}$, for $n = 1, 2, 3, \dots, N-1$ and $\forall (\mathbf{v}_h, \phi_{fh}, \phi_{wh}) \in V_h \times X_{fh} \times X_{wh}$, find $(\mathbf{u}_h^{n+1}, C_{fh}^{n+1}, C_{wh}^{n+1}) \in V_h \times X_{fh} \times X_{wh}$, such that

$$(18) \quad \left(\frac{3\mathbf{u}_h^{n+1} - 4\mathbf{u}_h^n + \mathbf{u}_h^{n-1}}{2\Delta t}, \mathbf{v}_h \right) + C^*(2\mathbf{u}_h^n - \mathbf{u}_h^{n-1}, \mathbf{u}_h^{n+1}, \mathbf{v}_h) + \nu(\nabla \mathbf{u}_h^{n+1}, \nabla \mathbf{v}_h) - (\nabla \cdot \mathbf{v}_h, p_h^{n+1}) = (\mathbf{f}^{n+1}, \mathbf{v}_h),$$

$$(19) \quad (\nabla \cdot \mathbf{u}_h^{n+1}, q) = 0,$$

$$(20) \quad \left(\frac{3C_{fh}^{n+1} - 4C_{fh}^n + C_{fh}^{n-1}}{2\Delta t}, \phi_{fh} \right) + b^*(2\mathbf{u}_h^n - \mathbf{u}_h^{n-1}, C_{fh}^{n+1}, \phi_{fh}) + (\mu_f \nabla C_{fh}^{n+1}, \nabla \phi_{fh}) + (C_{fh}^{n+1} - (2C_{wh}^n - C_{wh}^{n-1}), \phi_{fh})_\Gamma = (f_f^{n+1}, \phi_{fh}),$$

$$(21) \quad \left(\frac{3C_{wh}^{n+1} - 4C_{wh}^n + C_{wh}^{n-1}}{2\Delta t}, \phi_{wh} \right) + (\mu_w \nabla C_{wh}^{n+1}, \nabla \phi_{wh}) + (C_{wh}^{n+1} - (2C_{fh}^n - C_{fh}^{n-1}), \phi_{wh})_\Gamma = (f_w^{n+1}, \phi_{wh}).$$

4.2. Unconditional and long-time stability of the algorithm. In this subsection, we derive the unconditional and long-time stability of the BDF2 algorithm for the blood solute dynamics model.

Firstly, we report some important preliminaries and notations which are necessary for the estimation. The symmetric G-matrix can be defined as

$$G = \begin{pmatrix} \frac{1}{2} & -1 \\ -1 & \frac{5}{2} \end{pmatrix}$$

and its associated G-norm by $\|\chi\|_G^2 = (\chi, G\chi)$, $\forall \chi \in (L^2(\Omega))^2$.

By adapting the results from [50], the G-norm and the L^2 -norm are equivalent, where there $\exists c_u, c_l > 0$, such that

$$(22) \quad c_l \|\chi\|_G \leq \|\chi\| \leq c_u \|\chi\|_G.$$

To estimate the stability of the proposed algorithm, we introduce the following well-known lemmas.

Lemma 2. [50] Set $\chi^0 = [\mathbf{v}^0, \mathbf{v}^1]^T$ and $\chi^1 = [\mathbf{v}^1, \mathbf{v}^2]^T$. Then for any $\mathbf{v}^i \in L^2(\Omega)$, $i = 0, 1, 2$ the following relation holds

$$\left(\frac{3}{2}\mathbf{v}^2 - 2\mathbf{v}^1 + \frac{1}{2}\mathbf{v}^0, \mathbf{v}^2 \right) = \frac{1}{2}(\|\chi^1\|_G^2 - \|\chi^0\|_G^2) + \frac{1}{4} \|\mathbf{v}^2 - 2\mathbf{v}^1 + \mathbf{v}^0\|^2.$$

Lemma 3. Set $\chi^{n-1} = [\mathbf{v}^{n-1}, \mathbf{v}^n]^T$. Then for \mathbf{v}^n and $\mathbf{v}^{n-1} \in L^2(\Omega)$, we have

$$\|-2\mathbf{v}^n + \mathbf{v}^{n-1}\|^2 \leq 2 \|\chi^{n-1}\|_G^2.$$

Proof. Let $\chi^{n-1} = [\mathbf{v}^{n-1}, \mathbf{v}^n]^T$, such that $\mathbf{v}^{n-1}, \mathbf{v}^n \in L^2(\Omega)$.

We can write $(\chi^{n-1}, G\chi^{n-1})$ as follow

$$(\chi^{n-1}, G\chi^{n-1}) = \left(\begin{pmatrix} \mathbf{v}^{n-1} \\ \mathbf{v}^n \end{pmatrix}, \begin{pmatrix} \frac{1}{2} & -1 \\ -1 & \frac{5}{2} \end{pmatrix} \begin{pmatrix} \mathbf{v}^{n-1} \\ \mathbf{v}^n \end{pmatrix} \right),$$

$$\|\chi^{n-1}\|_G^2 = (\chi^{n-1}, G\chi^{n-1}) = \int \left(\frac{1}{2}\mathbf{v}^{n-1} - \mathbf{v}^n, -\mathbf{v}^{n-1} + \frac{5}{2}\mathbf{v}^n \right) (\mathbf{v}^{n-1}, \mathbf{v}^n)$$

$$\begin{aligned}
&= \frac{1}{2} \| \mathbf{v}^{n-1} \|^2 - 2(\mathbf{v}^{n-1}, \mathbf{v}^n) + \frac{5}{2} \| \mathbf{v}^n \|^2 \\
&= \frac{1}{2} (\| \mathbf{v}^{n-1} \|^2 - 4(\mathbf{v}^{n-1}, \mathbf{v}^n) + 4 \| \mathbf{v}^n \|^2) + \frac{1}{2} \| \mathbf{v}^n \|^2 \\
&= \frac{1}{2} (\| 2\mathbf{v}^n - \mathbf{v}^{n-1} \|^2 + \| \mathbf{v}^n \|^2) \\
&\geq \frac{1}{2} \| 2\mathbf{v}^n - \mathbf{v}^{n-1} \|^2,
\end{aligned}$$

hence, we complete the proof. \square

For convenience, some mathematical notations are provided

$$(23) \quad D\mathbf{v}^{n+1} = \frac{3}{2}\mathbf{v}^{n+1} - 2\mathbf{v}^n + \frac{1}{2}\mathbf{v}^{n-1}, \quad \delta\mathbf{v}^{n+1} = \mathbf{v}^{n+1} - 2\mathbf{v}^n + \mathbf{v}^{n-1}.$$

4.3. Unconditional stability of the BDF2 algorithm.

Theorem 1. *The proposed second-order backward differentiation decoupled algorithm BDF2 (18)-(21) is unconditionally stable on $(0, T]$ and satisfies*

$$\mathcal{B}^n + \mathcal{M}^n \leq (1 + c_1 \Delta t)(\mathcal{B}^{n-1} + \mathcal{M}^{n-1}) + \frac{c_{pf}^2 \Delta t}{\nu} \| \mathbf{f}^{n+1} \|^2 + \frac{3c_p^2 \Delta t}{\alpha} \| f_{fw}^{n+1} \|^2,$$

where

$$\begin{aligned}
\mathcal{B}^n &= \| \omega_u^n \|^2_G + \frac{\nu \Delta t}{4} \| \nabla \mathbf{u}^{n+1} \|^2, \\
\mathcal{M}^n &= \| \omega^n \|^2_G + \frac{\alpha \Delta t}{1 + c_1 \Delta t} \| \nabla C_{fw}^{n+1} \|^2 + \frac{\alpha \Delta t}{3(1 + c_1 \Delta t)} \| \nabla C_{fw}^n \|^2, \\
c_1 &= \frac{81c_{trf}^4 c_{trw}^4}{\alpha^3} \quad \alpha = \min\{\mu_f, \mu_w\}.
\end{aligned}$$

Proof. For the sake of simplicity, we drop the index identifying the mesh size h . Plugging $\mathbf{v} = 2\Delta t \mathbf{u}^{n+1}$ into the equation (18) and $q = 2\Delta t p^{n+1}$ into the equation (19). After that by using Lemma 2, Cauchy-Schwarz inequality and Young's inequality, we can get

$$\begin{aligned}
&\| \omega_u^n \|^2_G - \| \omega_u^{n-1} \|^2_G + \frac{1}{2} \| \delta \mathbf{u}^{n+1} \|^2 + 2\nu \Delta t \| \nabla \mathbf{u}^{n+1} \|^2 \\
(24) \quad &\leq \frac{c_{pf}^2 \Delta t}{\nu} \| \mathbf{f}^{n+1} \|^2 + \nu \Delta t \| \nabla \mathbf{u}^{n+1} \|^2,
\end{aligned}$$

such that $\omega_u^n = [\mathbf{u}^n, \mathbf{u}^{n-1}]^T$.

Remove the non-negative term $\frac{1}{2} \| \delta \mathbf{u}^{n+1} \|^2$ and add $\frac{\nu \Delta t}{4} \| \nabla \mathbf{u}^n \|^2$ on the both sides of (24), we get

$$\begin{aligned}
&(\| \omega_u^n \|^2_G + \frac{\nu \Delta t}{4} \| \nabla \mathbf{u}^{n+1} \|^2) + \frac{3\nu \Delta t}{4} \| \nabla \mathbf{u}^{n+1} \|^2 + \frac{\nu \Delta t}{4} \| \nabla \mathbf{u}^n \|^2 \\
(25) \quad &\leq (\| \omega_u^{n-1} \|^2_G + \frac{\nu \Delta t}{4} \| \nabla \mathbf{u}^n \|^2) + \frac{c_{pf}^2 \Delta t}{\nu} \| \mathbf{f}^{n+1} \|^2.
\end{aligned}$$

Let $\mathcal{B}^n = \| \omega_u^n \|^2_G + \frac{\nu \Delta t}{4} \| \nabla \mathbf{u}^{n+1} \|^2$, then

$$(26) \quad \mathcal{B}^n \leq \mathcal{B}^{n-1} + \frac{c_{pf}^2 \Delta t}{\nu} \| \mathbf{f}^{n+1} \|^2.$$

To estimate (20) – (21), firstly, we denote $C_{fw}^n = (C_f^n, C_w^n)$, $\phi_{fw}^n = (\phi_f^n, \phi_w^n) \in X_h = X_{fh} \times X_{wh}$ and $f_{fw}^n = (f_f^n, f_w^n)$. Setting $\phi_f = C_f^{n+1}$ in (20) and $\phi_w = C_w^{n+1}$ in (21), we get

$$\begin{aligned} & \left(\frac{3C_{fw}^{n+1} - 4C_{fw}^n + C_{fw}^{n-1}}{2\Delta t}, C_{fw}^{n+1} \right) + (\mu_f \nabla C_f^{n+1}, \nabla C_f^{n+1}) + (\mu_w \nabla C_w^{n+1}, \nabla C_w^{n+1}) \\ & + \left(C_f^{n+1} - (2C_w^n - C_w^{n-1}), C_f^{n+1} \right)_\Gamma + \left(C_w^{n+1} - (2C_f^n - C_f^{n-1}), C_w^{n+1} \right)_\Gamma \\ & = (f_{fw}^{n+1}, C_{fw}^{n+1}). \end{aligned} \quad (27)$$

Multiplying by $2\Delta t$ both sides of (27) and using Lemma 2, we obtain

$$\begin{aligned} & \| \omega^n \|_G^2 - \| \omega^{n-1} \|_G^2 + \frac{1}{2} \| \delta C_{fw}^{n+1} \|^2 + 2\Delta t (\mu_f \nabla C_f^{n+1}, \nabla C_f^{n+1}) \\ & + 2\Delta t (\mu_w \nabla C_w^{n+1}, \nabla C_w^{n+1}) + 2\Delta t \| C_{fw}^{n+1} \|^2_\Gamma \\ & = 2\Delta t (f_{fw}^{n+1}, C_{fw}^{n+1}) + 2\Delta t (2C_w^n - C_w^{n-1}, C_f^{n+1})_\Gamma + 2\Delta t (2C_f^n - C_f^{n-1}, C_w^{n+1})_\Gamma, \end{aligned} \quad (28)$$

where $\omega^n = [C_{fw}^n, C_{fw}^{n-1}]^\top$. Moreover, the bilinear terms satisfy

$$\begin{aligned} & (\mu_f \nabla C_f^{n+1}, \nabla C_f^{n+1}) + (\mu_w \nabla C_w^{n+1}, \nabla C_w^{n+1}) \\ & \geq \alpha \left(\| \nabla C_f^{n+1} \|^2 + \| \nabla C_w^{n+1} \|^2 \right) = \alpha \| \nabla C_{fw}^{n+1} \|^2, \end{aligned} \quad (29)$$

with $\alpha = \min\{\mu_f, \mu_w\}$.

Now we bound the right-hand side of (28). For the interface terms, we use Cauchy-Schwarz inequality and trace inequality to get

$$\begin{aligned} & 2\Delta t (2C_w^n - C_w^{n-1}, C_f^{n+1})_\Gamma + 2\Delta t (2C_f^n - C_f^{n-1}, C_w^{n+1})_\Gamma \\ & \leq 2\Delta t \left(\| 2C_w^n - C_w^{n-1} \|_\Gamma \| C_f^{n+1} \|_\Gamma + \| 2C_f^n - C_f^{n-1} \|_\Gamma \| C_w^{n+1} \|_\Gamma \right) \\ & \leq 2c_{trf} c_{trw} \Delta t \left(\| 2C_w^n - C_w^{n-1} \|^\frac{1}{2} \| 2\nabla C_w^n - \nabla C_w^{n-1} \|^\frac{1}{2} \| \nabla C_f^{n+1} \| \right. \\ & \quad \left. + \| 2C_f^n - C_f^{n-1} \|^\frac{1}{2} \| 2\nabla C_f^n - \nabla C_f^{n-1} \|^\frac{1}{2} \| \nabla C_w^{n+1} \| \right) \\ & \leq 2c_{trf} c_{trw} \Delta t \left(\| 2C_w^n - C_w^{n-1} \|^\frac{1}{2} (\sqrt{2} \| \nabla C_w^n \|^\frac{1}{2} + \| \nabla C_w^{n-1} \|^\frac{1}{2}) \| \nabla C_f^{n+1} \| \right. \\ & \quad \left. + \| 2C_f^n - C_f^{n-1} \|^\frac{1}{2} (\sqrt{2} \| \nabla C_f^n \|^\frac{1}{2} + \| \nabla C_f^{n-1} \|^\frac{1}{2}) \| \nabla C_w^{n+1} \| \right) \\ & = 2c_{trf} c_{trw} \Delta t (I_1 + I_2 + I_3 + I_4). \end{aligned} \quad (30)$$

Using Young's inequality and Lemma 3, each term of the right-hand side of (30) can be bounded as

$$\begin{aligned} I_1 & = \sqrt{2} \| 2C_w^n - C_w^{n-1} \|^\frac{1}{2} \| \nabla C_w^n \|^\frac{1}{2} \| \nabla C_f^{n+1} \| \\ & \leq \frac{\epsilon}{6} \| \nabla C_f^{n+1} \|^2 + \frac{27}{4\epsilon^3} \| 2C_w^n - C_w^{n-1} \|^2 + \frac{\epsilon}{3} \| \nabla C_w^n \|^2 \\ & \leq \frac{\epsilon}{6} \| \nabla C_f^{n+1} \|^2 + \frac{27}{2\epsilon^3} \| \omega^n \|_G^2 + \frac{\epsilon}{3} \| \nabla C_w^n \|^2, \end{aligned}$$

$$\begin{aligned} I_2 & = \| 2C_w^n - C_w^{n-1} \|^\frac{1}{2} \| \nabla C_w^{n-1} \|^\frac{1}{2} \| \nabla C_f^{n+1} \| \\ & \leq \frac{\epsilon}{6} \| \nabla C_f^{n+1} \|^2 + \frac{27}{8\epsilon^3} \| 2C_w^n - C_w^{n-1} \|^2 + \frac{\epsilon}{6} \| \nabla C_w^{n-1} \|^2 \end{aligned}$$

$$\leq \frac{\epsilon}{6} \|\nabla C_f^{n+1}\|^2 + \frac{27}{4\epsilon^3} \|\omega^n\|_G^2 + \frac{\epsilon}{6} \|\nabla C_w^{n-1}\|^2.$$

Similar for I_3 and I_4

$$\begin{aligned} I_3 &= \sqrt{2} \|2C_f^n - C_f^{n-1}\|^{\frac{1}{2}} \|\nabla C_f^n\|^{\frac{1}{2}} \|\nabla C_w^{n+1}\| \\ &\leq \frac{\epsilon}{6} \|\nabla C_w^{n+1}\|^2 + \frac{27}{2\epsilon^3} \|\omega^n\|^2 + \frac{\epsilon}{3} \|\nabla C_f^n\|^2, \\ I_4 &= \|2C_f^n - C_f^{n-1}\|^{\frac{1}{2}} \|\nabla C_f^{n-1}\|^{\frac{1}{2}} \|\nabla C_w^{n+1}\| \\ &\leq \frac{\epsilon}{6} \|\nabla C_w^{n+1}\|^2 + \frac{27}{4\epsilon^3} \|\omega^n\|_G^2 + \frac{\epsilon}{6} \|\nabla C_f^{n-1}\|^2. \end{aligned}$$

Choosing $\epsilon = \frac{\alpha}{c_{trf}c_{trw}}$ and combining the above inequalities with the equation (30), yields

$$\begin{aligned} &2\Delta t(2C_w^n - C_w^{n-1}, C_f^{n+1})_\Gamma + 2\Delta t(2C_f^n - C_f^{n-1}, C_w^{n+1})_\Gamma \\ &\leq \frac{81c_{trf}^4 c_{trw}^4 \Delta t}{\alpha^3} \|\omega^n\|_G^2 + \frac{2\alpha\Delta t}{3} \|\nabla C_{fw}^{n+1}\|^2 \\ (31) \quad &+ \frac{2\alpha\Delta t}{3} \|\nabla C_{fw}^n\|^2 + \frac{\alpha\Delta t}{3} \|\nabla C_{fw}^{n-1}\|^2. \end{aligned}$$

For the forcing terms, we use Cauchy-Schwarz inequality, Poincaré inequality and Young's inequality

$$(32) \quad 2\Delta t(f_{fw}^{n+1}, C_{fw}^{n+1}) \leq \frac{3c_p^2 \Delta t}{\alpha} \|f_{fw}^{n+1}\|^2 + \frac{\alpha\Delta t}{3} \|\nabla C_{fw}^{n+1}\|^2.$$

Substituting the above estimates in (28) and drop the non-negative terms $\frac{1}{2} \|\delta C_{fw}^{n+1}\|^2$ and $2\Delta t \|C_{fw}^{n+1}\|_\Gamma^2$, we get

$$\begin{aligned} \|\omega^n\|_G^2 + 2\alpha\Delta t \|\nabla C_{fw}^{n+1}\|^2 &\leq \left(1 + \frac{81c_{trf}^4 c_{trw}^4 \Delta t}{\alpha^3}\right) \|\omega^{n-1}\|_G^2 + \frac{2\alpha\Delta t}{3} \|\nabla C_{fw}^{n+1}\|^2 \\ &\quad + \frac{2\alpha\Delta t}{3} \|\nabla C_{fw}^n\|^2 + \frac{\alpha\Delta t}{3} \|\nabla C_{fw}^{n-1}\|^2 \\ (33) \quad &+ \frac{\alpha\Delta t}{3} \|\nabla C_{fw}^{n+1}\|^2 + \frac{3c_p^2 \Delta t}{\alpha} \|f_{fw}^{n+1}\|^2. \end{aligned}$$

Now adding $\frac{\alpha\Delta t}{3} \|\nabla C_{fw}^n\|^2$ on the both sides of (33), we have

$$\begin{aligned} &\|\omega^n\|_G^2 + \alpha\Delta t \|\nabla C_{fw}^{n+1}\|^2 + \frac{\alpha\Delta t}{3} \|\nabla C_{fw}^n\|^2 \\ &\leq \left(1 + \frac{81c_{trf}^4 c_{trw}^4 \Delta t}{\alpha^3}\right) \|\omega^{n-1}\|_G^2 + \alpha\Delta t \|\nabla C_{fw}^n\|^2 \\ (34) \quad &+ \frac{\alpha\Delta t}{3} \|\nabla C_{fw}^{n-1}\|^2 + \frac{3c_p^2 \Delta t}{\alpha} \|f_{fw}^{n+1}\|^2. \end{aligned}$$

Setting the following term $\mathcal{M}^n = \|\omega^n\|_G^2 + \frac{\alpha\Delta t}{1+c_1\Delta t} \|\nabla C_{fw}^{n+1}\|^2 + \frac{\alpha\Delta t}{3(1+c_1\Delta t)} \|\nabla C_{fw}^n\|^2$, where $c_1 = \frac{81c_{trf}^4 c_{trw}^4}{\alpha^3}$, the above inequality can be rewritten as

$$\mathcal{M}^n + \frac{\alpha\Delta t c_1}{1+c_1\Delta t} \|\nabla C_{fw}^{n+1}\|^2 + \frac{\alpha\Delta t c_1}{3(1+c_1\Delta t)} \|\nabla C_{fw}^n\|^2$$

$$(35) \quad \leq (1 + c_1 \Delta t) \mathcal{M}^{n-1} + \frac{3c_p^2 \Delta t}{\alpha} \| f_{fw}^{n+1} \|^2.$$

Neglecting all the positive terms from the left-hand side of (35), we get

$$(36) \quad \mathcal{M}^n \leq (1 + c_1 \Delta t) \mathcal{M}^{n-1} + \frac{3c_p^2 \Delta t}{\alpha} \| f_{fw}^{n+1} \|^2.$$

Combining (26) and (36) to get

$$\mathcal{B}^n + \mathcal{M}^n \leq (1 + c_1 \Delta t) (\mathcal{B}^{n-1} + \mathcal{M}^{n-1}) + \frac{c_{pf}^2 \Delta t}{\nu} \| \mathbf{f}^{n+1} \|^2 + \frac{3c_p^2 \Delta t}{\alpha} \| f_{fw}^{n+1} \|^2,$$

hence, the proof is completed. \square

4.4. The long-time stability of the BDF2 scheme.

Theorem 2. Assume that the time step restriction $\Delta t \leq \frac{\alpha^3}{384c_{trf}^4 c_{trw}^4}$ is satisfied, then the solution of the BDF2 scheme (18) – (21) is uniformly bounded over $0 \leq t^n < \infty$.

Proof. The derivation of the long-time stability of the second-order decoupled backward differentiation scheme for the incompressible Navier-Stokes equations can be found in [43]. Hence, we omit the detail derivation of (18) – (19) herein. On the other hand, we derive the long-time stability of the advection-diffusion equation and pure diffusion equation (20) – (21) for the blood solute dynamics model. To prove the long-time stability, we add and subtract new terms in the interface term, (27) becomes

$$(37) \quad \begin{aligned} & \| \omega^n \|_G^2 - \| \omega^{n-1} \|_G^2 + \frac{1}{2} \| \delta C_{fw}^{n+1} \|^2 \\ & + 2\Delta t (\mu_f \nabla C_f^{n+1}, \nabla C_f^{n+1}) + 2\Delta t (\mu_w \nabla C_w^{n+1}, \nabla C_w^{n+1}) \\ & + (C_f^{n+1}, C_f^{n+1})_\Gamma + (C_w^{n+1} - 2C_w^n + C_w^{n-1}, C_f^{n+1})_\Gamma - (C_w^{n+1}, C_f^{n+1})_\Gamma \\ & + (C_w^{n+1}, C_w^{n+1})_\Gamma + (C_f^{n+1} - 2C_f^n + C_f^{n-1}, C_w^{n+1})_\Gamma - (C_f^{n+1}, C_w^{n+1})_\Gamma \\ & = 2\Delta t (f_{fw}^{n+1}, C_{fw}^{n+1}). \end{aligned}$$

Rearranging the terms of (37), we get

$$(38) \quad \begin{aligned} & \| \omega^n \|_G^2 - \| \omega^{n-1} \|_G^2 + \frac{1}{2} \| \delta C_{fw}^{n+1} \|^2 + 2\Delta t (\mu_f \nabla C_f^{n+1}, \nabla C_f^{n+1}) \\ & + 2\Delta t (\mu_w \nabla C_w^{n+1}, \nabla C_w^{n+1}) + 2\Delta t \| C_f^{n+1} - C_w^{n+1} \|_\Gamma^2 \\ & = 2\Delta t (f_{fw}^{n+1}, C_{fw}^{n+1}) - 2\Delta t (\delta C_w^{n+1}, C_f^{n+1})_\Gamma - 2\Delta t (\delta C_f^{n+1}, C_w^{n+1})_\Gamma. \end{aligned}$$

Estimate the terms of the right-hand side of (38) by using Cauchy-Schwarz inequality, trace inequality and Young's inequality on the interface terms

$$(39) \quad \begin{aligned} -2\Delta t (\delta C_f^{n+1}, C_w^{n+1})_\Gamma & \leq 2\Delta t \| \delta C_f^{n+1} \|_\Gamma \| C_w^{n+1} \|_\Gamma \\ & \leq 2c_{trf} c_{trw} \Delta t \| \delta C_f^{n+1} \|^\frac{1}{2} \| \nabla \delta C_f^{n+1} \|^\frac{1}{2} \| \nabla C_w^{n+1} \| \\ & \leq 2c_{trf} c_{trw} \Delta t \| \delta C_f^{n+1} \|^\frac{1}{2} \left(\| \nabla C_f^{n+1} \|^\frac{1}{2} \right. \\ & \quad \left. + \sqrt{2} \| \nabla C_f^n \|^\frac{1}{2} + \| \nabla C_f^{n-1} \|^\frac{1}{2} \right) \| \nabla C_w^{n+1} \|. \end{aligned}$$

Each terms of the right-hand side of the equation (39) are bounded by applying Young's inequality

$$\| \delta C_f^{n+1} \|^\frac{1}{2} \| \nabla C_f^{n+1} \|^\frac{1}{2} \| \nabla C_w^{n+1} \|$$

$$(40) \quad \leq \frac{\epsilon}{8} \|\nabla C_w^{n+1}\|^2 + \frac{\epsilon}{16} \|\nabla C_f^{n+1}\|^2 + \frac{16}{\epsilon^3} \|\delta C_f^{n+1}\|^2,$$

$$(41) \quad \begin{aligned} & \sqrt{2} \|\delta C_f^{n+1}\|^{\frac{1}{2}} \|\nabla C_f^n\|^{\frac{1}{2}} \|\nabla C_w^{n+1}\| \\ & \leq \frac{\epsilon}{8} \|\nabla C_w^{n+1}\|^2 + \frac{\epsilon}{16} \|\nabla C_f^n\|^2 + \frac{64}{\epsilon^3} \|\delta C_f^{n+1}\|^2, \end{aligned}$$

$$(42) \quad \begin{aligned} & \|\delta C_f^{n+1}\|^{\frac{1}{2}} \|\nabla C_f^{n-1}\|^{\frac{1}{2}} \|\nabla C_w^{n+1}\| \\ & \leq \frac{\epsilon}{8} \|\nabla C_w^{n+1}\|^2 + \frac{\epsilon}{16} \|\nabla C_f^{n-1}\|^2 + \frac{16}{\epsilon^3} \|\delta C_f^{n+1}\|^2. \end{aligned}$$

We can obtain the similar estimations for the term $-2\Delta t(\delta C_w^{n+1}, C_f^{n+1})_\Gamma$ as just derived for $-2\Delta t(\delta C_f^{n+1}, C_w^{n+1})_\Gamma$ in the equation (39). Combining the estimations of $-2\Delta t(\delta C_f^{n+1}, C_w^{n+1})_\Gamma$ and $-2\Delta t(\delta C_w^{n+1}, C_f^{n+1})_\Gamma$ and setting $\epsilon = \frac{\alpha}{c_{trf}c_{trw}}$, we can obtain

$$\begin{aligned} & -2\Delta t((\delta C_f^{n+1}, C_w^{n+1})_\Gamma + (\delta C_w^{n+1}, C_f^{n+1})_\Gamma) \\ & \leq \frac{7\alpha\Delta t}{8} \|\nabla C_f^{n+1}\|^2 + \frac{7\alpha\Delta t}{8} \|\nabla C_w^{n+1}\|^2 \\ & \quad + \frac{\alpha\Delta t}{8} (\|\nabla C_f^n\|^2 + \|\nabla C_f^{n-1}\|^2 + \|\nabla C_w^n\|^2 + \|\nabla C_w^{n-1}\|^2) \\ & \quad + \frac{192c_{tr}^4c_{tw}^4\Delta t}{\alpha^3} \|\delta C_f^{n+1}\|^2 + \frac{192c_{trf}^4c_{trw}^4\Delta t}{\alpha^3} \|\delta C_w^{n+1}\|^2 \\ & = \frac{7\alpha\Delta t}{8} \|\nabla C_{fw}^{n+1}\|^2 + \frac{\alpha\Delta t}{8} (\|\nabla C_{fw}^n\|^2 + \|\nabla C_{fw}^{n-1}\|^2) \\ & \quad + \frac{192c_{trf}^4c_{trw}^4\Delta t}{\alpha^3} \|\delta C_{fw}^{n+1}\|^2. \end{aligned} \quad (43)$$

By using Poincaré inequality and Young's inequality, the forcing term can be bounded as

$$(44) \quad -2\Delta t(f_{fw}^{n+1}, C_{fw}^{n+1}) \leq \frac{8c_p^2\Delta t}{\alpha} \|f_{fw}^{n+1}\|^2 + \frac{\alpha\Delta t}{8} \|\nabla C_{fw}^{n+1}\|^2.$$

Substituting (43) and (44) into (38) and drop the non-negative term $2\Delta t \|\nabla C_f^{n+1} - C_w^{n+1}\|_\Gamma^2$, provides

$$\begin{aligned} & \|\omega^n\|_G^2 + \left(\frac{1}{2} - \frac{192c_{trf}^4c_{trw}^4\Delta t}{\alpha^3}\right) \|\delta C_{fw}^{n+1}\|^2 + \alpha\Delta t \|\nabla C_{fw}^{n+1}\|^2 \\ & \leq \|\omega^{n-1}\|_G^2 + \frac{\alpha\Delta t}{8} \|\nabla C_{fw}^n\|^2 + \frac{\alpha\Delta t}{8} \|\nabla C_{fw}^{n-1}\|^2 + \frac{8c_p^2\Delta t}{\alpha} \|f_{fw}^{n+1}\|^2. \end{aligned}$$

If the time step Δt satisfied the following restriction

$$(45) \quad \Delta t \leq \frac{\alpha^3}{384c_{trf}^4c_{trw}^4},$$

then

$$(46) \quad \begin{aligned} & \|\omega^n\|_G^2 + \alpha\Delta t \|\nabla C_{fw}^{n+1}\|^2 \\ & \leq \|\omega^{n-1}\|_G^2 + \frac{\alpha\Delta t}{8} \|\nabla C_{fw}^n\|^2 + \frac{\alpha\Delta t}{8} \|\nabla C_{fw}^{n-1}\|^2 + \frac{8c_p^2\Delta t}{\alpha} \|f_{fw}^{n+1}\|^2. \end{aligned}$$

Adding $\frac{3\alpha\Delta t}{8} \|\nabla C_{fw}^n\|^2$ on the both sides of the inequality (46) yields

$$(47) \quad \begin{aligned} & \|\omega^n\|_G^2 + \alpha\Delta t \|\nabla C_{fw}^{n+1}\|^2 + \frac{3\alpha\Delta t}{8} \|\nabla C_{fw}^n\|^2 \\ & \leq \|\omega^{n-1}\|_G^2 + \frac{\alpha\Delta t}{2} \|\nabla C_{fw}^n\|^2 + \frac{\alpha\Delta t}{8} \|\nabla C_{fw}^{n-1}\|^2 + \frac{8c_p^2\Delta t}{\alpha} \|f_{fw}^{n+1}\|^2. \end{aligned}$$

Set $\mathcal{M}^n = \|\omega^n\|_G^2 + \frac{\alpha\Delta t}{2} \|\nabla C_{fw}^{n+1}\|^2 + \frac{\alpha\Delta t}{8} \|\nabla C_{fw}^n\|^2$, then the above inequality can be bounded in the following way

$$(48) \quad \mathcal{M}^n + \frac{\alpha\Delta t}{2} \|\nabla C_{fw}^{n+1}\|^2 + \frac{\alpha\Delta t}{4} \|\nabla C_{fw}^n\|^2 \leq \mathcal{M}^{n-1} + \frac{8c_p^2\Delta t}{\alpha} \|f_{fw}^{n+1}\|^2.$$

Using Poincaré inequality and the equivalence property of the L^2 -norm and the G-norm, the two terms of the left-hand side of (48) can be written as

$$(49) \quad \begin{aligned} & \frac{\alpha}{2} \|\nabla C_{fw}^{n+1}\|^2 + \frac{\alpha}{4} \|\nabla C_{fw}^n\|^2 \\ & \geq \frac{\alpha}{4} \|\nabla C_{fw}^{n+1}\|^2 + \frac{\alpha}{8} \|\nabla C_{fw}^n\|^2 + \frac{\alpha}{8c_p^2} (\|C_{fw}^{n+1}\|^2 + \|C_{fw}^n\|^2) \\ & \geq \frac{\alpha}{4} \|\nabla C_{fw}^{n+1}\|^2 + \frac{\alpha}{8} \|\nabla C_{fw}^n\|^2 + \frac{\alpha c_l^2}{8c_p^2} \|\omega^n\|_G^2 \\ & \geq \gamma^* \left(\|\omega^n\|_G^2 + \frac{\alpha\Delta t}{2} \|\nabla C_{fw}^{n+1}\|^2 + \frac{\alpha\Delta t}{8} \|\nabla C_{fw}^n\|^2 \right) \\ & = \gamma^* \mathcal{M}^n, \end{aligned}$$

where $\gamma^* = \min \left\{ \frac{\alpha c_l^2}{8c_p^2}, \frac{1}{2\Delta t} \right\}$. Replacing the above bound into (48), gives

$$(50) \quad (1 + \gamma^*\Delta t)\mathcal{M}^n \leq \mathcal{M}^{n-1} + \frac{8c_p^2\Delta t}{\alpha} \|f_{fw}^{n+1}\|^2.$$

By the induction argument, the inequality (50) can be written as

$$(51) \quad \mathcal{M}^n \leq (1 + \gamma^*\Delta t)^{-n} \mathcal{M}^0 + \frac{8c_p^2\Delta t}{\alpha} \|f_{fw}^{n+1}\|^2 \sum_{i=0}^{n-1} \left(\frac{1}{1 + \gamma^*\Delta t} \right)^i.$$

Since $\frac{1}{1 + \gamma^*\Delta t} < 1$ and $n \rightarrow \infty$, then

$$\begin{aligned} \sum_{i=0}^{n-1} \frac{1}{(1 + \gamma^*\Delta t)^i} &= 1 + \frac{1}{(1 + \gamma^*\Delta t)} + \dots + \frac{1}{(1 + \gamma^*\Delta t)^{n-1}} \\ &= \frac{1 - \left(\frac{1}{1 + \gamma^*\Delta t} \right)^n}{1 - \frac{1}{1 + \gamma^*\Delta t}} = \frac{1}{\gamma^*\Delta t} = \frac{1 + \gamma^*\Delta t}{\gamma^*\Delta t}. \end{aligned}$$

Plugging the above geometric series results and using the triangle inequality, the equivalence of the L^2 -norm and the G-norm in (51), we obtain

$$\begin{aligned} & \|C_{fw}^{n+1}\|^2 + \|C_{fw}^n\|^2 + \Delta t \|\nabla(C_{fw}^{n+1} + C_{fw}^n)\|^2 \\ & \leq \tilde{c}(1 + \gamma^*\Delta t)^{-n} \left(\|C_{fw}^0\|^2 + \Delta t \|\nabla C_{fw}^0\|^2 + \|C_{fw}^1\|^2 + \Delta t \|\nabla C_{fw}^1\|^2 \right) \\ & \quad + \frac{8c_p^2(1 + \gamma^*\Delta t)}{\alpha\gamma^*} \|f_{fw}^{n+1}\|^2, \end{aligned}$$

which illustrates the uniform stability. \square

5. Convergence analysis of the second-order backward differentiation partitioned time-stepping scheme

To illustrate the optimal error estimate, we assume that the exact solution of $(\mathbf{u}, p, C_f, C_w)$ satisfies the following regularity conditions

$$\mathbf{u} \in L^p(0, T, H^{k+1}(\Omega_f)), \mathbf{u}_{tt} \in L^p(0, T, H^{k+1}(\Omega_f)), \mathbf{u}_{ttt} \in L^p(0, T, H^1(\Omega_f)),$$

$$p \in L^p(0, T, L^2(\Omega_f)),$$

(52)

$$C_f \in L^p(0, T, H^{k+1}(\Omega_f)), C_{tt,f} \in L^p(0, T, H^{k+1}(\Omega_f)), C_{ttt,f} \in L^p(0, T, H^1(\Omega_f)),$$

(53)

$$C_w \in L^p(0, T, H^{k+1}(\Omega_w)), C_{tt,w} \in L^p(0, T, H^{k+1}(\Omega_w)),$$

$$C_{ttt,w} \in L^p(0, T, H^1(\Omega_w)), \quad p = 2, \infty.$$

Moreover, we introduce the following discrete norms

$$\begin{aligned} \| \| \mathbf{v} \| \|_{L^2(0,T,H^k(\Omega_f|w))}^2 &= \Delta t \sum_{n=0}^N \| \mathbf{v}^n \|_{H^k(\Omega_f|w)}^2, \\ \| \| \mathbf{v} \| \|_{L^\infty(0,T,H^k(\Omega_f|w))}^2 &= \max_{0 \leq n \leq N} \| \mathbf{v} \|_{H^k(\Omega_f|w)}, \end{aligned}$$

and define the following errors

$$\begin{aligned} e_u^{n+1} &= \mathbf{u}(t^{n+1}) - \phi_u + \phi_u - \mathbf{u}_f^{n+1} = \eta_u^{n+1} + \varphi_u^{n+1} \quad \forall \phi_u \in V, \\ e_f^{n+1} &= C_f(t^{n+1}) - \phi_f + \phi_f - C_f^{n+1} = \eta_f^{n+1} + \varphi_f^{n+1} \quad \forall \phi_f \in X_f, \\ e_w^{n+1} &= C_w(t^{n+1}) - \phi_w + \phi_w - C_w^{n+1} = \eta_w^{n+1} + \varphi_w^{n+1} \quad \forall \phi_w \in X_w. \end{aligned} \quad (54)$$

Theorem 3. Let \mathbf{u}, p, C_f and C_w are the exact solution of the solute dynamics model (1) – (10) holds the regularity assumptions (52) for $p = 2$, and if the time step restriction

$$\Delta t \leq \frac{\alpha^3}{384c_{trf}^4 c_{trw}^4}$$

holds, then the approximate solution of the scheme (18) – (21) satisfies the following error estimate

$$\begin{aligned} &\| e_u^{N+1} \|^2 + \| e_u^N \|^2 + \| e_{fw}^{N+1} \|^2 + \| e_{fw}^N \|^2 + \| \nabla e_u^{N+1} \|^2 + \| \nabla e_{fw}^{N+1} \|^2 \\ &+ \| \nabla e_{fw}^N \|^2 + \Delta t \sum_{n=0}^N \| \nabla(e_u^{n+1} + e_u^n) \|^2 + \Delta t \sum_{n=0}^N \| \nabla(e_{fw}^{n+1} + e_{fw}^n) \|^2 \\ (55) \quad &\leq \tilde{c}(\Delta t^4 + h^{2k}). \end{aligned}$$

Moreover, if the solution is long-time regular in the sense the solution satisfies the regularity assumptions (52) for $p = \infty$ and $T = \infty$, then for any $0 \leq t^n < \infty$, there exists a strictly positive constant \tilde{c} , such that

$$\begin{aligned} &\| e_u^{N+1} \|^2 + \| e_u^N \|^2 + \| e_{fw}^{N+1} \|^2 + \| e_{fw}^N \|^2 \\ &+ \| \nabla e_u^{N+1} \|^2 + \| \nabla e_{fw}^{N+1} \|^2 + \| \nabla e_{fw}^N \|^2 \\ &\leq \tilde{c}(1 + \gamma_{min})^{-n} \left(\| \varphi_u^1 \|^2 + \| \varphi_u^0 \|^2 + \| \varphi_{fw}^1 \|^2 + \| \varphi_{fw}^0 \|^2 \right. \\ &\quad \left. + \Delta t \| \nabla \varphi_u^1 \|^2 + \Delta t \| \nabla \varphi_{fw}^1 \|^2 + \Delta t \| \nabla \varphi_{fw}^0 \|^2 \right) \end{aligned}$$

$$(56) \quad + \tilde{c}(\Delta t^4 + h^{2k}).$$

Proof. To derive the convergence analysis of the blood solute dynamics model, firstly, we deduce the error estimates for the Navier-Stokes equations. Secondly, we derive the error estimate of the advection-diffusion and pure diffusion equation.

Consider the proposed *BDF2* scheme (18) – (21) over the discretely divergence free space $W_h = \{\mathbf{v}_h \in V_h : (\nabla \cdot \mathbf{v}_h, q_h) = 0, \forall q_h \in Q_h\}$, instead of V_h , which lead to vanish the pressure term $(p^{n+1}, \nabla \cdot \mathbf{v})$. Subtracting (18) from (11) and (19) from (12) at $t = t^{n+1}$, gives us the following error equation

$$\begin{aligned} & \frac{1}{\Delta t} (D e_u^{n+1}, \mathbf{v}) + \nu (\nabla e_u^{n+1}, \mathbf{v}) - (p(t^{n+1}), \nabla \cdot \mathbf{v}) \\ & + C^*(\mathbf{u}(t^{n+1}), \mathbf{u}(t^{n+1}), \mathbf{v}) - C^*(2\mathbf{u}^n - \mathbf{u}^{n-1}, \mathbf{u}^{n+1}, \mathbf{v}) \\ (57) \quad & = -(r_u^{n+1}, \mathbf{v}), \end{aligned}$$

$$(58) \quad (\nabla \cdot (\mathbf{u}(t^{n+1}) - \mathbf{u}^{n+1}), q) = 0,$$

$$\text{where } r_u^{n+1} = \mathbf{u}_t(t^{n+1}) - \frac{1}{\Delta t} D \mathbf{u}(t^{n+1}).$$

For all $\mathbf{v} \in W_h$ and any $\lambda \in W_h$, we have

$$(59) \quad (p(t^{n+1}), \nabla \cdot \mathbf{v}) = (p(t^{n+1}) - \lambda^{n+1}, \nabla \cdot \mathbf{v}).$$

Thus

$$\begin{aligned} & \frac{1}{\Delta t} (D \varphi_u^{n+1}, \mathbf{v}) + \nu (\nabla \varphi_u^{n+1}, \nabla \mathbf{v}) \\ & = -(r_u^{n+1}, \mathbf{v}) - \frac{1}{\Delta t} (D \eta_u^{n+1}, \mathbf{v}) - \nu (\nabla \eta_u^{n+1}, \nabla \mathbf{v}) \\ & \quad - C^*(\mathbf{u}(t^{n+1}), \mathbf{u}(t^{n+1}), \mathbf{v}) + C^*(2\mathbf{u}^n - \mathbf{u}^{n-1}, \mathbf{u}^{n+1}, \mathbf{v}) \\ (60) \quad & \quad + (p(t^{n+1}) - \lambda^{n+1}, \nabla \cdot \mathbf{v}). \end{aligned}$$

Plugging $\mathbf{v} = \varphi_u^{n+1}$ and $q = \varphi_p^{n+1}$ into the equation (60), we get

$$\begin{aligned} & \frac{1}{\Delta t} (D \varphi_u^{n+1}, \varphi_u^{n+1}) + \nu (\nabla \varphi_u^{n+1}, \nabla \varphi_u^{n+1}) \\ & = -(r_u^{n+1}, \varphi_u^{n+1}) - \frac{1}{\Delta t} (D \eta_u^{n+1}, \varphi_u^{n+1}) - \nu (\nabla \eta_u^{n+1}, \nabla \varphi_u^{n+1}) \\ & \quad - C^*(\mathbf{u}(t^{n+1}), \mathbf{u}(t^{n+1}), \varphi_u^{n+1}) + C^*(2\mathbf{u}^n - \mathbf{u}^{n-1}, \mathbf{u}^{n+1}, \varphi_u^{n+1}) \\ (61) \quad & \quad + (p(t^{n+1}) - \lambda^{n+1}, \nabla \cdot \varphi_u^{n+1}). \end{aligned}$$

Multiplying both sides of equation (61) by 2 and using Lemma 2, we obtain

$$\begin{aligned} & \frac{1}{\Delta t} \left(\| \chi_u^n \|^2 - \| \chi_u^{n-1} \|^2 + \frac{1}{2} \| \delta \varphi_u^{n+1} \|^2 \right) + 2\nu \| \nabla \varphi_u^{n+1} \|^2 \\ & = -2(r_u^{n+1}, \varphi_u^{n+1}) - \frac{2}{\Delta t} (D \eta_u^{n+1}, \varphi_u^{n+1}) - 2\nu (\nabla \eta_u^{n+1}, \varphi_u^{n+1}) \\ & \quad - 2C^*(\mathbf{u}(t^{n+1}), \mathbf{u}(t^{n+1}), \varphi_u^{n+1}) + 2C^*(2\mathbf{u}^n - \mathbf{u}^{n-1}, \mathbf{u}^{n+1}, \varphi_u^{n+1}) \\ (62) \quad & \quad + 2(p(t^{n+1}) - \lambda^{n+1}, \nabla \cdot \varphi_u^{n+1}), \end{aligned}$$

with $\chi_u^n = [\varphi_u^{n+1}, \varphi_u^n]^T$.

Next, we estimate each term of the right-hand side of equation (62) one by one. Using Cauchy-Schwarz inequality and Young's inequality, we obtain

$$(63) \quad -2(r_u^{n+1}, \varphi_u^{n+1}) \leq \frac{8c_{pf}^2}{\nu} \| r_u^{n+1} \|^2 + \frac{\nu}{8} \| \nabla \varphi_u^{n+1} \|^2,$$

$$(64) \quad -\frac{2}{\Delta t}(D\eta_u^{n+1}, \varphi_u^{n+1}) \leq \frac{8c_{pf}^2}{\nu} \|\frac{1}{\Delta t}D\eta_u^{n+1}\|^2 + \frac{\nu}{8}\|\nabla\varphi_u^{n+1}\|^2,$$

$$(65) \quad -2\nu(\nabla\eta_u^{n+1}, \varphi_u^{n+1}) \leq 8\nu c_{pf}^2 \|\nabla\eta_u^{n+1}\|^2 + \frac{\nu}{8}\|\nabla\varphi_u^{n+1}\|^2.$$

Using the approximation properties (17), and the following inequality: for sufficiently small $h \leq h_1$ with $Ch_1^{\frac{1}{2}} \leq C_1$, and by using the inverse inequality $\|\mathbf{v}_h\|_{m,q} \leq Ch^{l-m+n(\frac{1}{q}-\frac{1}{p})}\|\mathbf{v}_h\|_{l,p}$, there holds

$$\begin{aligned} \|\nabla\eta_u^{n+1}\|_{L^3} &\leq Ch^{-1+3(\frac{1}{3}-\frac{1}{2})}\|\eta_u^{n+1}\|_{L^2} \\ &\leq Ch^{-\frac{3}{2}}\|\eta_u^{n+1}\|_{L^2} \\ &\leq Ch^{\frac{1}{2}} \leq C_1. \end{aligned}$$

thus, the trilinear terms can be estimated as

$$\begin{aligned} &-2C^*(\mathbf{u}(t^{n+1}), \mathbf{u}(t^{n+1}), \varphi_u^{n+1}) + 2C^*(2\mathbf{u}^n - \mathbf{u}^{n-1}, \mathbf{u}^{n+1}, \varphi_u^{n+1}) \\ &= -2C^*(\mathbf{u}(t^{n+1}), \mathbf{u}(t^{n+1}), \varphi_u^{n+1}) + 2C^*(\mathbf{u}(t^{n+1}), \mathbf{u}^{n+1}, \varphi_u^{n+1}) - 2C^*(\mathbf{u}(t^{n+1}) \\ &\quad - 2\mathbf{u}^n + \mathbf{u}^{n-1}, \mathbf{u}^{n+1}, \varphi_u^{n+1}) \\ &= -2C^*(\mathbf{u}(t^{n+1}), \mathbf{u}(t^{n+1}) - \mathbf{u}^{n+1}, \varphi_u^{n+1}) \\ &\quad - 2C^*(\mathbf{u}(t^{n+1}) + \mathbf{u}^{n+1} - \mathbf{u}^{n+1} - 2\mathbf{u}^n + \mathbf{u}^{n-1}, \mathbf{u}^{n+1}, \varphi_u^{n+1}) \\ &= -2C^*(\mathbf{u}(t^{n+1}), \eta_u^{n+1}, \varphi_u^{n+1}) \\ &\quad - 2C^*(\mathbf{u}(t^{n+1}) - \mathbf{u}^{n+1}, \mathbf{u}^{n+1}, \varphi_u^{n+1}) - 2C^*(\delta\mathbf{u}^{n+1}, \mathbf{u}^{n+1}, \varphi_u^{n+1}) \\ &= -2C^*(\mathbf{u}(t^{n+1}), \eta_u^{n+1}, \varphi_u^{n+1}) + 2C^*(\mathbf{u}(t^{n+1}) - \mathbf{u}^{n+1}, \eta_u^{n+1}, \varphi_u^{n+1}) \\ &\quad - 2C^*(\mathbf{u}(t^{n+1}) - \mathbf{u}^{n+1}, \mathbf{u}(t^{n+1}), \varphi_u^{n+1}) + 2C^*(\delta\mathbf{u}^{n+1}, \eta_u^{n+1}, \varphi_u^{n+1}) \\ &\quad - 2C^*(\delta\mathbf{u}^{n+1}, \mathbf{u}(t^{n+1}), \varphi_u^{n+1}) + 2C^*(\delta\mathbf{u}(t^{n+1}), \eta_u^{n+1}, \varphi_u^{n+1}) \\ &\quad - 2C^*(\delta\mathbf{u}(t^{n+1}), \eta_u^{n+1}, \varphi_u^{n+1}) \\ &= -2C^*(\mathbf{u}(t^{n+1}), \eta_u^{n+1}, \varphi_u^{n+1}) + 2C^*(\mathbf{u}(t^{n+1}) - \mathbf{u}^{n+1}, \eta_u^{n+1}, \varphi_u^{n+1}) \\ &\quad - 2C^*(\mathbf{u}(t^{n+1}) - \mathbf{u}^{n+1}, \mathbf{u}(t^{n+1}), \varphi_u^{n+1}) + 2C^*(\delta(\mathbf{u}(t^{n+1}) - \mathbf{u}^{n+1}), \eta_u^{n+1}, \varphi_u^{n+1}) \\ &\quad - 2C^*(\delta(\mathbf{u}(t^{n+1}) - \mathbf{u}^{n+1}), \mathbf{u}(t^{n+1}), \varphi_u^{n+1}) - 2C^*(\delta\mathbf{u}(t^{n+1}), \eta_u^{n+1}, \varphi_u^{n+1}) \\ &\quad + 2C^*(\delta\mathbf{u}(t^{n+1}), \mathbf{u}(t^{n+1}), \varphi_u^{n+1}) \\ &\leq \bar{c}(\|\mathbf{u}(t^{n+1})\|_{L^4}\|\nabla\eta_u^{n+1}\|_{L^2}\|\varphi_u^{n+1}\|_{L^4} + \|\mathbf{u}(t^{n+1}) - \mathbf{u}^{n+1}\|_{L^2}\|\nabla\eta_u^{n+1}\|_{L^3}\|\varphi_u^{n+1}\|_{L^6} \\ &\quad + \|\mathbf{u}(t^{n+1}) - \mathbf{u}^{n+1}\|_{L^2}\|\nabla\mathbf{u}(t^{n+1})\|_{L^3}\|\varphi_u^{n+1}\|_{L^6} \\ &\quad + \|\delta(\mathbf{u}(t^{n+1}) - \mathbf{u}^{n+1})\|_{L^2}\|\nabla\eta_u^{n+1}\|_{L^3}\|\varphi_u^{n+1}\|_{L^6} \\ &\quad + \|\delta(\mathbf{u}(t^{n+1}) - \mathbf{u}^{n+1})\|_{L^2}\|\nabla\mathbf{u}(t^{n+1})\|_{L^3}\|\varphi_u^{n+1}\|_{L^6} \\ &\quad + \|\delta\mathbf{u}(t^{n+1})\|_{L^2}\|\nabla\eta_u^{n+1}\|_{L^3}\|\varphi_u^{n+1}\|_{L^6} \\ &\quad + \|\delta\mathbf{u}(t^{n+1})\|_{L^3}\|\nabla\mathbf{u}(t^{n+1})\|_{L^2}\|\varphi_u^{n+1}\|_{L^6}) \\ &\leq C_1^2(\|\eta_u^{n+1}\|^2 + \|\varphi_u^{n+1}\|^2 + \|\delta\eta_u^{n+1}\|^2 + \|\delta\varphi_u^{n+1}\|^2) \\ &\quad + \bar{c}(\|\nabla\eta_u^{n+1}\|^2 + \|\delta\mathbf{u}(t^{n+1})\|^2) + \frac{\nu}{16}\|\nabla\varphi_u^{n+1}\|^2. \end{aligned} \tag{66}$$

The last term can be bounded as

$$2\left(p(t^{n+1}) - \lambda^{n+1}, \nabla \cdot \varphi_u^{n+1}\right) \leq \|p(t^{n+1}) - \lambda^{n+1}\| \|\nabla \cdot \varphi_u^{n+1}\|$$

$$(67) \quad \leq \frac{16d}{\nu} \| p(t^{n+1}) - \lambda^{n+1} \|^2 + \frac{\nu}{16} \| \nabla \varphi_u^{n+1} \|^2.$$

Plugging the above estimates (63) – (67) into the equation (62), to obtain

$$\begin{aligned} & \| \chi_u^n \|^2 - \| \chi_u^{n-1} \|^2 + \left(\frac{1}{2} - C_1^2 \Delta t \right) \| \delta \varphi_u^{n+1} \|^2 + \frac{3\nu\Delta t}{2} \| \nabla \varphi_u^{n+1} \|^2 \\ & \leq \frac{4c_{pf}^2 \Delta t}{\nu} \| r_u^{n+1} \|^2 + \frac{4c_{pf}^2 \Delta t}{\nu} \| \frac{1}{\Delta t} D \eta_u^{n+1} \|^2 \\ & \quad + (4\nu c_{pf}^2 + \bar{c}) \Delta t \| \nabla \eta_u^{n+1} \|^2 + \bar{c} \Delta t \| \delta \mathbf{u}(t^{n+1}) \|^2 \\ (68) \quad & \quad + \frac{16d\Delta t}{\nu} \| p(t^{n+1}) - \lambda^{n+1} \|^2 + C_1^2 \Delta t (\| \eta_u^{n+1} \|^2 + \| \varphi_u^{n+1} \|^2 + \| \delta \eta_u^{n+1} \|^2). \end{aligned}$$

Adding $\frac{\nu\Delta t}{4} \| \nabla \varphi_u^n \|^2$ on the both sides of the above inequality and rearranging the terms to achieve

$$\begin{aligned} & \mathcal{A}^n + \left(\frac{1}{2} - C_1^2 \Delta t \right) \| \delta \varphi_u^{n+1} \|^2 + \frac{\mu\Delta t}{4} (\| \nabla \varphi_u^{n+1} \|^2 + \| \nabla \varphi_u^n \|^2) + \nu\Delta t \| \nabla \varphi_u^{n+1} \|^2 \\ & \leq \mathcal{A}^{n-1} + \frac{4c_{pf}^2 \Delta t}{\nu} \| r_u^{n+1} \|^2 + \frac{4c_{pf}^2 \Delta t}{\nu} \| \frac{1}{\Delta t} D \eta_u^{n+1} \|^2 \\ & \quad + (4\nu c_{pf}^2 + \bar{c}) \Delta t \| \nabla \eta_u^{n+1} \|^2 + \bar{c} \Delta t \| \delta \mathbf{u}(t^{n+1}) \|^2 \\ (69) \quad & \quad + \frac{16d\Delta t}{\nu} \| p(t^{n+1}) - \lambda^{n+1} \|^2 + C_1^2 \Delta t (\| \eta_u^{n+1} \|^2 + \| \varphi_u^{n+1} \|^2 + \| \delta \eta_u^{n+1} \|^2). \end{aligned}$$

such that $\mathcal{A}^n = \| \chi_u^n \|^2 + \frac{\nu\Delta t}{4} \| \nabla \varphi_u^{n+1} \|^2$.

In the following, we derive the convergence analysis for the advection-diffusion equation and pure diffusion equation of the blood solute dynamics model.

Subtracting (20) and (21) from (13) and (14), the error equation can be constructed as

$$\begin{aligned} & \frac{1}{\Delta t} (D e_{fw}^{n+1}, \phi_{fw}) + \mu_f (\nabla e_f^{n+1}, \nabla \phi_f) \\ & + \mu_w (\nabla e_w^{n+1}, \nabla \phi_w) + C^*(u(t^{n+1}), C_f(t^{n+1}), \phi_f) \\ & - C^*(2u^n - u^{n-1}, C_f^{n+1}, \phi_f) + (e_f^{n+1}, \phi_f)_\Gamma - (C_w(t^{n+1}) - 2C_w^n + C_w^{n-1}, \phi_f)_\Gamma \\ & + (e_w^{n+1}, \phi_w)_\Gamma - (C_f(t^{n+1}) - 2C_f^n + C_f^{n-1}, \phi_w)_\Gamma \\ (70) \quad & = - (r_{fw}^{n+1}, \phi_{fw}), \end{aligned}$$

where

$$r_{fw}^{n+1} = (r_f^{n+1}, r_w^{n+1}), \quad r_i^{n+1} = C_{t,i}(t^{n+1}) - \frac{1}{\Delta t} D C_i(t^{n+1}), \quad \text{for } i = f, w.$$

Using (54), choosing $\phi_f^{n+1} = \varphi_f^{n+1}$ and $\phi_w = \varphi_w^{n+1}$, adding and subtracting the terms $(C_f^{n+1}, \varphi_w^{n+1})_\Gamma$ and $(C_w^{n+1}, \varphi_f^{n+1})_\Gamma$, the error equation (70) can be rewritten as

$$\begin{aligned} & \frac{1}{\Delta t} (D \varphi_{fw}^{n+1}, \varphi_{fw}^{n+1}) + \mu_f (\nabla \varphi_f^{n+1}, \nabla \varphi_f^{n+1}) + \mu_w (\nabla \varphi_w^{n+1}, \nabla \varphi_w^{n+1}) \\ & + C^*(u(t^{n+1}), C_f(t^{n+1}), \varphi_f^{n+1}) - C^*(2u^n - u^{n-1}, C_f^{n+1}, \varphi_f^{n+1}) + (\varphi_f^{n+1}, \varphi_f^{n+1})_\Gamma \\ & + (\varphi_w^{n+1}, \varphi_w^{n+1})_\Gamma + (\eta_f^{n+1}, \varphi_f^{n+1})_\Gamma + (\eta_w^{n+1}, \varphi_w^{n+1})_\Gamma \\ & - (\varphi_w^{n+1}, \varphi_f^{n+1})_\Gamma - (\eta_w^{n+1}, \varphi_f^{n+1})_\Gamma \end{aligned}$$

$$\begin{aligned}
& -(\varphi_f^{n+1}, \varphi_w^{n+1})_\Gamma - (\eta_f^{n+1}, \varphi_w^{n+1})_\Gamma - (\delta C_w^{n+1}, \varphi_f^{n+1})_\Gamma - (\delta C_f^{n+1}, \varphi_w^{n+1})_\Gamma \\
(71) \quad & = -(r_{fw}^{n+1}, \varphi_{fw}) - \frac{1}{\Delta t} (D\eta_{fw}^{n+1}, \varphi_{fw}^{n+1}) - \mu_f (\nabla \eta_f^{n+1}, \nabla \varphi_f^{n+1}) - \mu_w (\nabla \eta_w^{n+1}, \nabla \varphi_w^{n+1}).
\end{aligned}$$

Multiplying both sides of equation (71) by 2, using Lemma 2, adding and subtracting the term $2(\nabla C_f(t^{n+1}), \varphi_w^{n+1})_\Gamma$, we get

$$\begin{aligned}
& \frac{1}{\Delta t} (\|\chi^n\|_G^2 - \|\chi^{n-1}\|_G^2 + \frac{1}{2} \|\delta\varphi_{fw}^{n+1}\|^2) \\
& + 2\alpha \|\nabla\varphi_{fw}^{n+1}\|^2 + 2\|\varphi_f^{n+1} - \varphi_w^{n+1}\|_\Gamma^2 \\
& \leq -2(r_{fw}^{n+1}, \phi_{fw}) - \frac{2}{\Delta t} (D\eta_{fw}^{n+1}, \varphi_{fw}^{n+1}) - 2\alpha (\nabla \eta_{fw}^{n+1}, \nabla \varphi_{fw}^{n+1}) \\
& + 2(\eta_w^{n+1} - \eta_f^{n+1}, \varphi_f^{n+1} - \varphi_w^{n+1})_\Gamma - 2C^*(u(t^{n+1}), C_f(t^{n+1}), \phi_f^{n+1}) \\
& + 2C^*(2u^n - u^{n-1}, C_f^{n+1}, \phi_f^{n+1}) + 2(\delta C_w(t^{n+1}), \varphi_f^{n+1})_\Gamma + 2(\delta C_f(t^{n+1}), \varphi_w^{n+1})_\Gamma \\
(72) \quad & - 2(\delta\varphi_f^{n+1}, \varphi_w^{n+1})_\Gamma - 2(\delta\varphi_w^{n+1}, \varphi_f^{n+1})_\Gamma - 2(\delta\eta_f^{n+1}, \varphi_w^{n+1})_\Gamma - 2(\delta\eta_w^{n+1}, \varphi_f^{n+1})_\Gamma,
\end{aligned}$$

where $\chi^n = [\varphi_{fw}^{n+1}, \varphi_{fw}^n]^T$.

Estimate the terms involving the right-hand side of the above inequality one by one, we obtain

$$(73) \quad -2(r_{fw}^{n+1}, \varphi_{fw}) \leq \frac{c_p^2}{\varepsilon_{fw}} \|r_{fw}^{n+1}\|^2 + \varepsilon_{fw} \|\nabla\varphi_{fw}^{n+1}\|^2,$$

$$(74) \quad -\frac{2}{\Delta t} (D\eta_{fw}^{n+1}, \varphi_{fw}^{n+1}) \leq \frac{c_p^2}{\varepsilon_{fw}} \left\| \frac{1}{\Delta t} D\eta_{fw}^{n+1} \right\|^2 + \varepsilon_{fw} \|\nabla\varphi_{fw}^{n+1}\|^2,$$

$$(75) \quad -2\alpha (\nabla \eta_{fw}^{n+1}, \nabla \varphi_{fw}^{n+1}) \leq \frac{1}{\varepsilon_{fw}} \|\nabla \eta_{fw}^{n+1}\|^2 + \varepsilon_{fw} \|\nabla \varphi_{fw}^{n+1}\|^2.$$

To estimate the interface terms, we use Cauchy-Schwarz inequality and trace inequality

$$\begin{aligned}
& 2(\eta_f^{n+1}, \varphi_f^{n+1})_\Gamma + 2(\eta_w^{n+1}, \varphi_w^{n+1})_\Gamma - 2(\eta_w^{n+1}, \varphi_f^{n+1})_\Gamma - 2(\eta_f^{n+1}, \varphi_w^{n+1})_\Gamma \\
& \leq 2\|\eta_f^{n+1}\|_\Gamma \|\varphi_f^{n+1}\|_\Gamma + 2\|\eta_w^{n+1}\|_\Gamma \|\varphi_w^{n+1}\|_\Gamma \\
& \quad + 2\|\eta_w^{n+1}\|_\Gamma \|\varphi_f^{n+1}\|_\Gamma + 2\|\eta_f^{n+1}\|_\Gamma \|\varphi_w^{n+1}\|_\Gamma \\
& \leq 2c_{trf}^2 \|\nabla \eta_f^{n+1}\| \|\nabla \varphi_f^{n+1}\| + 2c_{trw}^2 \|\nabla \eta_w^{n+1}\| \|\nabla \varphi_w^{n+1}\| \\
& \quad + 2c_{trf} c_{trw} \|\nabla \eta_w^{n+1}\| \|\nabla \varphi_f^{n+1}\| + 2c_{trf} c_{trw} \|\nabla \eta_f^{n+1}\| \|\nabla \varphi_w^{n+1}\| \\
& \leq \frac{2c_{trf}^4}{\varepsilon_{fw}} \|\nabla \eta_f^{n+1}\|^2 + \frac{\varepsilon_{fw}}{2} \|\nabla \varphi_f^{n+1}\|^2 + \frac{2c_{trw}^4}{\varepsilon_{fw}} \|\nabla \eta_w^{n+1}\|^2 + \frac{\varepsilon_{fw}}{2} \|\nabla \varphi_w^{n+1}\|^2 \\
& \quad + \frac{2c_{trf}^2 c_{trw}^2}{\varepsilon_{fw}} \|\nabla \eta_w^{n+1}\|^2 + \frac{\varepsilon_{fw}}{2} \|\nabla \varphi_f^{n+1}\|^2 \\
& \quad + \frac{2c_{trf}^2 c_{trw}^2}{\varepsilon_{fw}} \|\nabla \eta_f^{n+1}\|^2 + \frac{\varepsilon_{fw}}{2} \|\nabla \varphi_w^{n+1}\|^2 \\
& \leq \frac{2c_{trf}^4}{\varepsilon_{fw}} \|\nabla \eta_f^{n+1}\|^2 + \frac{2c_{trw}^4}{\varepsilon_{fw}} \|\nabla \eta_w^{n+1}\|^2
\end{aligned}$$

$$(76) \quad + \frac{2c_{trf}^2 c_{trw}^2}{\varepsilon_{fw}} \|\nabla \eta_{fw}^{n+1}\|^2 + \varepsilon_{fw} \|\nabla \varphi_{fw}^{n+1}\|^2.$$

And

$$(77) \quad \begin{aligned} 2(\delta C_w(t^{n+1}), \varphi_f^{n+1})_\Gamma &\leq 2 \|\delta C_w(t^{n+1})\|_\Gamma \|\varphi_f^{n+1}\|_\Gamma \\ &\leq \frac{c_{trf}^2 c_{trw}^2}{\varepsilon_{fw}} \|\nabla \delta C_w(t^{n+1})\|^2 + \varepsilon_{fw} \|\nabla \varphi_f^{n+1}\|^2. \end{aligned}$$

Also

$$(78) \quad \begin{aligned} 2(\delta C_f(t^{n+1}), \varphi_w^{n+1})_\Gamma &\leq 2 \|\delta C_f(t^{n+1})\|_\Gamma \|\varphi_w^{n+1}\|_\Gamma \\ &\leq \frac{c_{trf}^2 c_{trw}^2}{\varepsilon_{fw}} \|\nabla \delta C_f(t^{n+1})\|^2 + \varepsilon_{fw} \|\nabla \varphi_w^{n+1}\|^2. \end{aligned}$$

In the similar way, we achieve

$$(79) \quad -2(\delta \eta_f^{n+1}, \varphi_w^{n+1})_\Gamma \leq \frac{c_{trf}^2 c_{trw}^2}{\varepsilon_{fw}} \|\nabla \delta \eta_f^{n+1}\|^2 + \varepsilon_{fw} \|\nabla \varphi_w^{n+1}\|^2,$$

$$(80) \quad -2(\delta \eta_{fw}^{n+1}, \varphi_f^{n+1})_\Gamma \leq \frac{c_{trf}^2 c_{trw}^2}{\varepsilon_{fw}} \|\nabla \delta \eta_{fw}^{n+1}\|^2 + \varepsilon_{fw} \|\nabla \varphi_f^{n+1}\|^2.$$

Adapting the similar techniques as illustrated in (39)–(41), the two interface terms can be bounded by

$$(81) \quad \begin{aligned} &2(\delta \varphi_f^{n+1}, \varphi_w^{n+1})_\Gamma + 2(\delta \varphi_w^{n+1}, \varphi_f^{n+1})_\Gamma \\ &\leq \frac{7\alpha}{8} \|\nabla \varphi_{fw}^{n+1}\|^2 + \frac{\alpha}{8} \left(\|\nabla \varphi_{fw}^n\|^2 + \|\nabla \varphi_{fw}^{n-1}\|^2 \right) + \frac{192c_{tr}^4 c_{tw}^4}{\alpha^3} \|\delta \varphi_{fw}^{n+1}\|^2. \end{aligned}$$

By the same technique in (66), we have

$$(82) \quad \begin{aligned} &-2(b^*(\mathbf{u}(t^{n+1}), C_f(t^{n+1}), \varphi_f^{n+1}) - b^*(2\mathbf{u}^n - \mathbf{u}^{n-1}, C_f^{n+1}, \varphi_f^{n+1})) \\ &\leq C_1^2 (\|\eta_u^{n+1}\|^2 + \|\varphi_u^{n+1}\|^2 + \|\delta \eta_u^{n+1}\|^2 + \|\delta \varphi_u^{n+1}\|^2) \\ &+ \bar{c} (\|\nabla \eta_f^{n+1}\|^2 + \|\delta \mathbf{u}(t^{n+1})\|^2) + \epsilon_{fw} \|\nabla \varphi_f^{n+1}\|^2. \end{aligned}$$

Plugging the above estimates (73)–(82) into the equation (72) and taking $\epsilon_{fw} = \frac{\alpha}{72}$, to achieve

$$(83) \quad \begin{aligned} &\|\chi^n\|_G^2 + \left(\frac{1}{2} - \frac{192c_{tr}^3 c_{tw}^3 \Delta t}{\alpha^3} \right) \|\delta \varphi_{fw}^{n+1}\|^2 \\ &+ \alpha \Delta t \|\nabla \varphi_{fw}^{n+1}\|^2 + 2\Delta t \|\varphi_f^{n+1} - \varphi_w^{n+1}\|_\Gamma^2 \\ &\leq \|\chi^{n-1}\|_G^2 + \frac{\alpha \Delta t}{8} (\|\nabla \varphi_{fw}^n\|^2 + \|\nabla \varphi_{fw}^{n-1}\|^2) \\ &+ c \left(\Delta t \|r_{fw}^{n+1}\|^2 + \Delta t \left\| \frac{1}{\Delta t} D \eta_{fw}^{n+1} \right\|^2 \right. \\ &+ \Delta t \|\nabla \eta_{fw}^{n+1}\|^2 + \Delta t \|\nabla \delta C_{fw}(t^{n+1})\|^2 \\ &+ \Delta t \|\nabla \delta \eta_{fw}^{n+1}\|^2 + \|\delta \mathbf{u}(t^{n+1})\|^2 \Big) + \frac{\nu \Delta t}{2} \|\nabla \varphi_u^{n+1}\|^2 \\ &+ C_1^2 \Delta t (\|\eta_u^{n+1}\|^2 + \|\varphi_u^{n+1}\|^2 + \|\delta \eta_u^{n+1}\|^2 + \|\delta \varphi_u^{n+1}\|^2) \\ &+ \bar{c} \Delta t (\|\nabla \eta_f^{n+1}\|^2 + \|\delta \mathbf{u}(t^{n+1})\|^2). \end{aligned}$$

If the time step restriction $\Delta t \leq \frac{\alpha^3}{384c_{trf}^4 c_{trw}^4}$ is satisfied and by dropping the non-negative term $2\Delta t \|\varphi_f^{n+1} - \varphi_w^{n+1}\|_\Gamma^2$, yields

$$\begin{aligned}
& \|\chi^n\|_G^2 + \alpha\Delta t \|\nabla\varphi_{fw}^{n+1}\|^2 \\
\leq & \|\chi^{n-1}\|_G^2 + \frac{\alpha\Delta t}{8} (\|\nabla\varphi_{fw}^n\|^2 + \|\nabla\varphi_{fw}^{n-1}\|^2) \\
& + c \left(\Delta t \|r_{fw}^{n+1}\|^2 + \Delta t \left\| \frac{1}{\Delta t} D\eta_{fw}^{n+1} \right\|^2 \right. \\
& \left. + \Delta t \|\nabla\eta_{fw}^{n+1}\|^2 + \Delta t \|\nabla\delta C_{fw}(t^{n+1})\|^2 \right. \\
& \left. + \Delta t \|\nabla\delta\eta_{fw}^{n+1}\|^2 + \|\delta\mathbf{u}(t^{n+1})\|^2 \right) + \frac{\nu\Delta t}{2} \|\nabla\varphi_u^{n+1}\|^2 \\
& + C_1^2 \Delta t (\|\eta_u^{n+1}\|^2 + \|\varphi_u^{n+1}\|^2 + \|\delta\eta_u^{n+1}\|^2 + \|\delta\varphi_u^{n+1}\|^2) \\
(84) \quad & + \bar{c}\Delta t (\|\nabla\eta_f^{n+1}\|^2 + \|\delta\mathbf{u}(t^{n+1})\|^2).
\end{aligned}$$

Following the similar steps as in (48) to get

$$\begin{aligned}
& \mathcal{E}^n + \frac{\alpha\Delta t}{2} \|\nabla\varphi_{fw}^{n+1}\|^2 + \frac{\alpha\Delta t}{4} \|\nabla\varphi_{fw}^n\|^2 \\
\leq & \mathcal{E}^{n-1} + c \left(\Delta t \|r_{fw}^{n+1}\|^2 + \Delta t \left\| \frac{1}{\Delta t} D\eta_{fw}^{n+1} \right\|^2 \right. \\
& \left. + \Delta t \|\nabla\eta_{fw}^{n+1}\|^2 + \Delta t \|\nabla\delta C_{fw}(t^{n+1})\|^2 \right. \\
& \left. + \Delta t \|\nabla\delta\eta_{fw}^{n+1}\|^2 + \|\delta\mathbf{u}(t^{n+1})\|^2 \right) + \frac{\nu\Delta t}{2} \|\nabla\varphi_u^{n+1}\|^2 \\
& + C_1^2 \Delta t (\|\eta_u^{n+1}\|^2 + \|\varphi_u^{n+1}\|^2 + \|\delta\eta_u^{n+1}\|^2 + \|\delta\varphi_u^{n+1}\|^2) \\
(85) \quad & + \bar{c}\Delta t (\|\nabla\eta_f^{n+1}\|^2 + \|\delta\mathbf{u}(t^{n+1})\|^2).
\end{aligned}$$

where $\mathcal{E}^n = \|\chi^n\|_G^2 + \frac{\alpha\Delta t}{2} \|\nabla\varphi_{fw}^{n+1}\|^2 + \frac{\alpha\Delta t}{8} \|\nabla\varphi_{fw}^n\|^2$. Combining (69) and (85) and applying the triangle inequality, we obtain

$$\begin{aligned}
& \mathcal{A}^n + \mathcal{E}^n + \left(\frac{1}{2} - 2C_1^2 \Delta t \right) \|\delta\varphi_u^{n+1}\|^2 \\
& + \frac{3\Delta t}{2} \|\nabla(\varphi_u^{n+1} + \varphi_u^n)\|^2 + \frac{\alpha\Delta t}{4} \|\nabla(\varphi_{fw}^{n+1} + \varphi_{fw}^n)\|^2 \\
\leq & \mathcal{A}^{n-1} + \mathcal{E}^{n-1} + \tilde{c} \left(\Delta t \|r_u^{n+1}\|^2 \right. \\
& \left. + \Delta t \|r_{fw}^{n+1}\|^2 + \Delta t \left\| \frac{1}{\Delta t} D\eta_u^{n+1} \right\|^2 + \Delta t \left\| \frac{1}{\Delta t} D\eta_{fw}^{n+1} \right\|^2 \right. \\
& \left. + \Delta t \|\nabla\eta_u^{n+1}\|^2 + \Delta t \|\nabla\eta_{fw}^{n+1}\|^2 + \Delta t \|\nabla\mathbf{u}(t^{n+1})\|^2 \right. \\
& \left. + \Delta t \|\nabla\delta C_{fw}(t^{n+1})\|^2 + \Delta t \|\nabla\delta\eta_{fw}^{n+1}\|^2 + \frac{16d\Delta t}{\nu} \|p(t^{n+1}) - \lambda^{n+1}\|^2 \right) \\
(86) \quad & + C_1^2 \Delta t (\|\eta_u^{n+1}\|^2 + \|\varphi_u^{n+1}\|^2 + \|\delta\eta_u^{n+1}\|^2) + \bar{c}\Delta t (\|\nabla\eta_f^{n+1}\|^2 + \|\delta\mathbf{u}(t^{n+1})\|^2).
\end{aligned}$$

Now we estimate each term of the right-hand side of equation (86) one by one. By using Taylor expansion and the approximation properties (17), we get

$$(87) \quad \|r_u^{n+1}\|^2 \leq c_0 \Delta t^3 \int_{t^{n-1}}^{t^{n+1}} \|\mathbf{u}_{ttt}\|^2 dt \leq c_0 \Delta t^4 \|\mathbf{u}_{ttt}\|_{L^\infty(0, t^{n+1}, L^2)}^2.$$

$$(88) \quad \|r_{fw}^{n+1}\|^2 \leq c_0 \Delta t^3 \int_{t^{n-1}}^{t^{n+1}} \|C_{fw,ttt}\|^2 dt \leq c_0 \Delta t^4 \|C_{fw,ttt}\|_{L^\infty(0, t^{n+1}, L^2)}^2.$$

$$(89) \quad \begin{aligned} \| \delta \mathbf{u}(t^{n+1}) \|^2 &\leq c_0 \Delta t^3 \int_{t^{n-1}}^{t^{n+1}} \| \mathbf{u}_{ttt} \|^2 dt \\ &\leq c_0 \Delta t^4 \| \mathbf{u}_{ttt} \|_{L^\infty(0,t^{n+1},L^2)}^2. \end{aligned}$$

$$(90) \quad \begin{aligned} \| \nabla \delta C_{fw}(t^{n+1}) \|^2 &\leq c_0 \Delta t^3 \int_{t^{n-1}}^{t^{n+1}} \| \nabla C_{fw,ttt} \|^2 dt \\ &\leq c_0 \Delta t^4 \| \nabla C_{fw,ttt} \|_{L^\infty(0,t^{n+1},L^2)}^2. \end{aligned}$$

$$(91) \quad \begin{aligned} \| \frac{1}{\Delta t} D \eta_u^{n+1} \|^2 &\leq c_0 h^{2(k+1)} \| \frac{1}{\Delta t} D \mathbf{u}(t^{n+1}) \|_{H^{k+1}}^2 \\ &\leq \frac{c_0 h^{2(k+1)}}{\Delta t} \int_{t^{n-1}}^{t^{n+1}} \| \mathbf{u}_t \|_{H^{k+1}}^2 dt \\ &\leq c_0 h^{2(k+1)} \| \mathbf{u}_t \|_{L^\infty(0,t^{n+1},H^{k+1})}^2. \end{aligned}$$

$$(92) \quad \begin{aligned} \| \frac{1}{\Delta t} D \eta_{fw}^{n+1} \|^2 &\leq \frac{c_0 h^{2(k+1)}}{\Delta t} \int_{t^{n-1}}^{t^{n+1}} \| C_{fw,t} \|_{H^{k+1}}^2 dt \\ &\leq c_0 h^{2(k+1)} \| C_{fw,t} \|_{L^\infty(0,t^{n+1},H^{k+1})}^2. \end{aligned}$$

$$(93) \quad \begin{aligned} \| \nabla \delta \eta_u^{n+1} \|^2 &\leq c_0 h^{2k} \| \delta \mathbf{u}(t^{n+1}) \|_{H^{k+1}}^2 \\ &\leq c_0 h^{2k} \Delta t^3 \int_{t^{n-1}}^{t^{n+1}} \| \mathbf{u}_{tt} \|_{H^{k+1}}^2 dt \\ &\leq c_0 h^{2k} \Delta t^4 \| \mathbf{u}_{tt} \|_{L^\infty(0,t^{n+1},H^{k+1})}^2. \end{aligned}$$

$$(94) \quad \begin{aligned} \| \nabla \delta \eta_{fw}^{n+1} \|^2 &\leq c_0 h^{2k} \Delta t^3 \int_{t^{n-1}}^{t^{n+1}} \| C_{fw,tt} \|_{H^{k+1}}^2 dt \\ &\leq c_0 h^{2k} \Delta t^4 \| C_{fw,tt} \|_{L^\infty(0,t^{n+1},H^{k+1})}^2. \end{aligned}$$

$$(95) \quad \| \nabla \eta_u^{n+1} \|^2 \leq c_0 h^{2k} \| \mathbf{u}^{n+1} \|_{H^{k+1}}^2.$$

$$(96) \quad \| \nabla \eta_{fw}^{n+1} \|^2 \leq c_0 h^{2k} \| C_{fw}^{n+1} \|_{H^{k+1}}^2.$$

We bound the pressure term in the following way

$$(97) \quad \| p(t^{n+1}) - \lambda^{n+1} \|^2 \leq c_0 h^{2k} \| p \|_{H^k}^2.$$

By inserting (87)-(97) into (86), sum over 0 to $N-1$, we obtain

$$\begin{aligned} \mathcal{A}^N + \mathcal{E}^N + \frac{3\Delta t}{2} \sum_{n=0}^{N-1} \| \nabla(\varphi_u^{n+1} + \varphi_u^n) \|^2 + \frac{\alpha \Delta t}{4} \sum_{n=0}^{N-1} \| \nabla(\varphi_{fw}^{n+1} + \varphi_{fw}^n) \|^2 \\ \leq \mathcal{A}^0 + \mathcal{E}^0 + \tilde{c} \left(\Delta t^4 (\| \mathbf{u}_{ttt} \|_{L^2(0,t^N,L^2)}^2 + \| C_{fw,ttt} \|_{L^2(0,t^N,L^2)}^2) \right. \\ \left. + \Delta t^4 (\| \mathbf{u}_{ttt} \|_{L^2(0,t^N,L^2)}^2 + \| \nabla C_{fw,ttt} \|_{L^2(0,t^N,L^2)}^2) \right. \\ \left. + h^{2(k+1)} (\| \mathbf{u}_t \|_{L^2(0,t^N,H^{k+1})}^2 + \| C_{fw,t} \|_{L^2(0,t^N,H^{k+1})}^2) \right. \\ \left. + h^{2k} \Delta t^4 (\| \mathbf{u}_{tt} \|_{L^2(0,t^N,H^{k+1})}^2 + \| C_{fw,tt} \|_{L^2(0,t^N,H^{k+1})}^2) \right. \\ \left. + h^{2k} \| \mathbf{u} \|_{L^2(0,t^N,H^{k+1})}^2 + h^{2k} \| C_{fw} \|_{L^2(0,t^N,H^{k+1})}^2 \right) \end{aligned}$$

$$(98) \quad + h^{2k} \| p(t^{n+1}) \|_{L^2(0, t^N, H^k)}^2 \Big) + C_1^2 \Delta t \sum_{n=0}^{N-1} \|\varphi_u^{n+1}\|^2.$$

By the equivalence of the G-norm and L^2 -norm, we can get

$$\begin{aligned} & \|\varphi_u^{N+1}\|^2 + \|\varphi_u^N\|^2 + \|\varphi_{fw}^{N+1}\|^2 + \|\varphi_{fw}^N\|^2 + \|\nabla\varphi_u^{N+1}\|^2 + \|\nabla\varphi_{fw}^{N+1}\|^2 \\ & + \|\nabla\varphi_{fw}^N\|^2 + \Delta t \sum_{n=0}^N \|\nabla(\varphi_u^{n+1} + \varphi_u^n)\|^2 + \Delta t \sum_{n=0}^N \|\nabla(\varphi_{fw}^{n+1} + \varphi_{fw}^n)\|^2 \\ & \leq \tilde{c} \left(\|\varphi_u^1\|^2 + \|\varphi_u^0\|^2 + \|\varphi_{fw}^1\|^2 + \|\varphi_{fw}^0\|^2 + \Delta t \|\nabla\varphi_u^1\|^2 \right. \\ (99) \quad & \left. + \Delta t \|\nabla\varphi_{fw}^1\|^2 + \Delta t \|\nabla\varphi_{fw}^0\|^2 \right) + (\Delta t^4 + h^{2k}) + C_1^2 \Delta t \sum_{n=0}^{N-1} \|\varphi_u^{n+1}\|^2. \end{aligned}$$

By the Gronwall inequality and the triangle inequality, we get

$$\begin{aligned} & \|e_u^{N+1}\|^2 + \|e_u^N\|^2 + \|e_{fw}^{N+1}\|^2 + \|e_{fw}^N\|^2 + \|\nabla e_u^{N+1}\|^2 + \|\nabla e_{fw}^{N+1}\|^2 \\ & + \|\nabla e_{fw}^N\|^2 + \Delta t \sum_{n=0}^N \|\nabla(e_u^{n+1} + e_u^n)\|^2 + \Delta t \sum_{n=0}^N \|\nabla(e_{fw}^{n+1} + e_{fw}^n)\|^2 \\ & \leq \tilde{c} \left(\|\varphi_u^1\|^2 + \|\varphi_u^0\|^2 + \|\varphi_{fw}^1\|^2 + \|\varphi_{fw}^0\|^2 + \Delta t \|\nabla\varphi_u^1\|^2 \right. \\ (100) \quad & \left. + \Delta t \|\nabla\varphi_{fw}^1\|^2 + \Delta t \|\nabla\varphi_{fw}^0\|^2 \right) + (\Delta t^4 + h^{2k}). \end{aligned}$$

Long-time error estimate: To prove the long-time error estimate, we rewrite the terms on the left-hand side of (69) in the following way

$$\begin{aligned} & \frac{\mu\Delta t}{4} (\|\nabla\varphi_u^{n+1}\|^2 + \|\nabla\varphi_u^n\|^2) + \frac{\nu\Delta t}{2} \|\nabla\varphi_u^{n+1}\|^2 \\ & \geq \frac{\nu c_l^2 \Delta t}{4c_{pf}^2} \|\nabla\chi_u^{n+1}\|_G^2 + \frac{\nu\Delta t}{2} \|\nabla\varphi_u^{n+1}\|^2 \\ & \geq \gamma \left(\|\nabla\chi_u^{n+1}\|_G^2 + \frac{\mu\Delta t}{4} \|\nabla\varphi_u^{n+1}\|^2 \right) \\ (101) \quad & = \gamma \mathcal{A}^n, \end{aligned}$$

where $\gamma = \min\{2, \frac{\nu c_l^2 \Delta t}{4c_{pf}^2}\}$.

Substituting (101) into (69), we get

$$\begin{aligned} & (1 + \gamma) \mathcal{A}^n + \frac{1}{2} \|\delta\varphi_u^{n+1}\|^2 + \frac{\nu\Delta t}{2} \|\nabla\varphi_u^{n+1}\|^2 \\ & \leq \mathcal{A}^{n-1} + \frac{4c_{pf}^2 \Delta t}{\nu} \|r_u^{n+1}\|^2 \\ & \quad + \frac{4c_{pf}^2 \Delta t}{\nu} \left\| \frac{1}{\Delta t} D\eta_u^{n+1} \right\|^2 + (4\nu c_{pf}^2 + \bar{c}) \Delta t \|\nabla\eta_u^{n+1}\|^2 + \bar{c} \Delta t \|\delta\mathbf{u}(t^{n+1})\|^2 \\ & \quad + \frac{16d\Delta t}{\nu} \|\mathbf{p}(t^{n+1}) - \lambda^{n+1}\|^2 \\ (102) \quad & \quad + C_1^2 \Delta t (\|\eta_u^{n+1}\|^2 + \|\varphi_u^{n+1}\|^2 + \|\delta\eta_u^{n+1}\|^2 + \|\delta\varphi_u^{n+1}\|^2). \end{aligned}$$

Also, the two terms in the right-hand side of (85) can be estimated in the similar way as (49)

$$\begin{aligned}
 & \frac{\alpha\Delta t}{2} \|\nabla\varphi_{fw}^{n+1}\|^2 + \frac{\alpha\Delta t}{4} \|\nabla\varphi_{fw}^n\|^2 \\
 & \geq \gamma^* \left(\|\chi^n\|_G^2 + \frac{\alpha\Delta t}{2} \|\nabla\varphi_{fw}^{n+1}\|^2 + \frac{\alpha\Delta t}{8} \|\nabla\varphi_{fw}^n\|^2 \right) \\
 (103) \quad & = \gamma^* \mathcal{E}^n,
 \end{aligned}$$

such that $\gamma^* = \min\left\{\frac{\alpha c_l^2 \Delta t}{8c_p^2}, \frac{1}{2}\right\}$.

Then

$$\begin{aligned}
 (1 + \gamma^*) \mathcal{E}^n & \leq \mathcal{E}^{n-1} + c \left(\Delta t \|r_{fw}^{n+1}\|^2 + \Delta t \left\| \frac{1}{\Delta t} D\eta_{fw}^{n+1} \right\|^2 \right. \\
 & \quad + \Delta t \|\nabla\eta_{fw}^{n+1}\|^2 + \Delta t \|\nabla\delta C_{fw}(t^{n+1})\|^2 \\
 & \quad + \Delta t \|\nabla\delta\eta_{fw}^{n+1}\|^2 + \|\delta\mathbf{u}(t^{n+1})\|^2 \left. \right) + \frac{\nu\Delta t}{2} \|\nabla\varphi_u^{n+1}\|^2 \\
 & \quad + C_1^2 \Delta t (\|\eta_u^{n+1}\|^2 + \|\varphi_u^{n+1}\|^2 + \|\delta\eta_u^{n+1}\|^2 + \|\delta\varphi_u^{n+1}\|^2) \\
 (104) \quad & \quad + \bar{c} \Delta t (\|\nabla\eta_f^{n+1}\|^2 + \|\delta\mathbf{u}(t^{n+1})\|^2).
 \end{aligned}$$

Define $\gamma_{min} = \min\{\gamma, \gamma^*\}$, combine (102) and (104) and using (87) – (97)

$$\begin{aligned}
 (1 + \gamma_{min})(\mathcal{A}^n + \mathcal{E}^n) & + \left(\frac{1}{2} - 2C_1^2 \Delta t \right) \|\delta\varphi_u^{n+1}\|^2 \\
 & \leq (\mathcal{A}^{n-1} + \mathcal{E}^{n-1}) + \tilde{c} \Delta t \left(\Delta t^4 (\|\mathbf{u}_{ttt}\|_{L^\infty(0,\infty,L^2)}^2 + \|C_{fw,ttt}\|_{L^\infty(0,\infty,L^2)}^2) \right. \\
 & \quad + \Delta t^4 (\|\nabla\mathbf{u}_{tt}\|_{L^\infty(0,\infty,H^{k+1})}^2 + \|\nabla C_{fw,tt}\|_{L^\infty(0,\infty,H^{k+1})}^2) \\
 & \quad + h^{2(k+1)} (\|\mathbf{u}_t\|_{L^\infty(0,\infty,H^{k+1})}^2 + \|C_{fw,t}\|_{L^\infty(0,\infty,H^{k+1})}^2) \\
 & \quad + h^{2k} \Delta t^4 (\|\mathbf{u}_{tt}\|_{L^\infty(0,\infty,H^{k+1})}^2 + \|C_{fw,tt}\|_{L^\infty(0,\infty,H^{k+1})}^2) \left. \right) \\
 & \quad + h^{2k} (\|\mathbf{u}\|_{L^\infty(0,\infty,H^{k+1})}^2 + \|C_{fw}\|_{L^\infty(0,\infty,H^{k+1})}^2) \\
 (105) \quad & \quad + h^{2k} \|p(t^{n+1})\|_{L^\infty(0,\infty,H^k)}^2 + C_1^2 \Delta t \|\varphi_u^{n+1}\|^2.
 \end{aligned}$$

Then by induction argument, we get

$$(106) \quad \mathcal{A}^n + \mathcal{E}^n \leq (1 + \gamma_{min})^{-n} (\mathcal{A}^0 + \mathcal{E}^0) + \tilde{c} (\Delta t^4 + h^{2k}) + C_1^2 \Delta t \sum_{n=0}^{N-1} \|\varphi_u^{n+1}\|^2,$$

similarly by using the triangle inequality, we can achieve the long-time error estimate (56). \square

6. Numerical results

To illustrate the theoretical results, four numerical experiments are performed to show the validity and accuracy of the proposed algorithm. In the first example, we confirm the predicted convergence rates for the proposed scheme by taking the exact solution of the model problem. The second numerical test investigates the blood flow and solute behavior in the bifurcated artery, with and without stenosis. Moreover, we present the long-time stability of the BDF2 algorithm for the blood solute dynamics model. In the third example, we conduct numerical experiments on the double stenoses artery to present the impact of the permeability and shear stress on the concentration of the blood solute. The fourth example demonstrates

TABLE 1. Convergence performance of *BDF2* for fixed $\Delta t = 0.001$ at $T=1.0$.

h	$\ u(t^n) - u^n\ _1$	rate	$\ p(t^n) - p^n\ $	rate	$\ C_f(t^n) - C_f^n\ _1$	rate	$\ C_w(t^n) - C_w^n\ _1$	rate
1/4	0.047824000		0.091399300		0.003204570		0.00857860	
1/8	0.012148700	1.9769	0.020391500	2.1642	0.000687313	2.2210	0.00206354	2.0556
1/16	0.002752490	2.1419	0.004918160	2.0517	0.000166088	2.0490	0.000537018	1.9420
1/32	0.000606100	2.1831	0.001169130	2.0726	4.1498e-005	2.0008	0.000133321	2.0100
1/64	0.000164973	1.8773	0.000330698	1.8218	1.02211e-05	2.0214	3.27424e-005	2.0256

TABLE 2. Convergence performance of *BDF2* for time stepsize $\Delta t = h$ at $T = 1.0$.

Δt	$\ u(t^n) - u^n\ _1$	rate	$\ p(t^n) - p^n\ $	rate	$\ C_f(t^n) - C_f^n\ _1$	rate	$\ C_w(t^n) - C_w^n\ _1$	rate
1/10	0.005690610		0.010121200		0.000849795		0.001308850	
1/20	0.001632060	1.8018	0.002863090	1.8217	0.000213983	1.9896	0.000341998	1.9362
1/30	0.000678053	2.1663	0.001274040	1.9969	9.5982e-005	1.9773	0.000154399	1.9613
1/40	0.000399693	1.8371	0.000740176	1.8877	5.4146e-005	1.9899	8.72836e-005	1.9826
1/50	0.000266068	1.8236	0.000500251	1.7557	3.48286e-005	1.9774	5.81180e-005	1.8225
1/60	0.000185646	1.9740	0.000359595	1.8102	2.39885e-005	2.0450	3.92048e-005	2.1592
1/70	0.000129001	2.36145	0.000275997	1.71641	1.77227e-005	1.96385	2.94223e-005	1.86212
1/80	9.98899e-005	1.91531	0.000230029	1.36437	1.35649e-005	2.00222	2.26074e-005	1.97315
1/90	7.48173e-005	2.45383	0.000199417	1.21245	1.07254e-005	1.99411	1.81025e-005	1.88675

the effect of the dilation of the artery due to the abdominal aortic aneurysm on the blood flow. We use the well-known Taylor-Hood elements $P2 - P1$ for the fluid velocity and pressure, and the continuous piecewise quadratic function $P2$ for both concentration in the lumen and the arterial wall.

6.1. Convergence test. Let the domain Ω be composed of $\Omega_f = [0, 1] \times [0, 1]$ and $\Omega_w = [0, 1] \times [0, -1]$, with the common interface $\Gamma = [0, 1] \times \{0\}$. The below analytical solution satisfies the interface conditions:

$$\begin{aligned} u_1 &:= 10(x^2 - 2x^3 + x^2)(2y^3 - 3y^2 + y) \cos(t), \\ u_2 &:= -10(2x^3 - 3x^2 + x)(y^4 - 2y^3 + y^2) \cos(t), \\ p &:= 10(2x - 1)(2y - 1) \cos(t), \\ C_f &:= x(1 - x)(1 - y)e^{-t}, \\ C_w &:= x(1 - x)(2 - y - 3y^2)e^{-t}. \end{aligned}$$

The right-hand side data in the partial differential equations, initial conditions are chosen such that the true solution is satisfied. The parameters value are considered as: $\nu = 1.0$, $\mu_f = 1.0$, $\mu_w = 1.0$ and $\zeta = 1.0$.

In Tables 1, we compute the errors between the exact solution and the approximate solution for the proposed second-order backward differentiation scheme with final time $T = 1.0$, time-step size $\Delta t = 0.001$ and varying mesh size $h = 1/4, 1/8, 1/16, 1/32, 1/64$. The result shows that the optimal convergence order $O(h^2)$ is achieved for the velocity and concentration \mathbf{u}, C_f, C_w in H^1 -semi-norm and pressure p in L^2 -norm. On the other hand, we set $\Delta t = h$ and varying time step size, $\Delta t = 1/10, 1/20, 1/30, 1/40, 1/50, 1/60$. Table 2 shows that optimal convergence $O(\Delta t^2)$ is obtained in time for \mathbf{u}, C_f, C_w in H^1 -semi-norm and p in L^2 -norm.

6.2. The bifurcated artery with and without stenosis. The main reason for cardiovascular disease, including atherosclerosis, is to believe that the transport of the macromolecules, in particular “Low-Density Lipoprotein (LDL)”, from the lumen to the arterial wall leads to narrowing of the artery which disorder the smooth blood flowing. Thus the study of the blood behavior in the artery gives a better

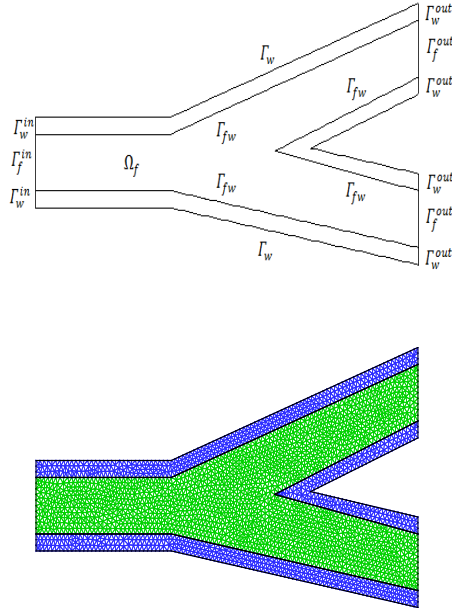


FIGURE 2. Left: a sketch of the simulation domain. Right: illustration of the computational mesh.

understanding of the relationship between the local features of the blood, the effect of the flow on the concentration of the macromolecules and the development of the pathologies [51, 52]. In this example, a 2D-simplified conceptual domain is considered to demonstrate the flow speed, streamlines, pressure field and concentration behavior in the lumen and the arterial wall, in both bifurcated arteries, with and without stenosis. On the other hand, we illustrate the effect of the development of the diseases on blood flow by taking different stenosis size [53, 54]. Furthermore, the long-time stability and consistency of the proposed scheme are presented.

The geometrical model for the lumen Ω_f and the wall Ω_w for the bifurcated artery are shown in Figure 2. The interface Γ_{fw} is defined as $\Gamma_{fw} = \{(x, y) : y = 1.5, 0 \leq x \leq 3.4\} \cup \{(x, y) : y = -1/6.2x + 10.84/6.2, 3.4 \leq x \leq 9.6\} \cup \{(x, y) : y = -0.7/3.6x + 12.12/3.6, 9.6 \leq x \leq 6.6\} \cup \{(x, y) : 1.3/3.6x + 0.12/3.6, 6.6 \leq x \leq 9.6\} \cup \{(x, y) : y = 1/3.1x + 4.35/3.1, 9.6 \leq x \leq 3.4\} \cup \{(x, y) : y = 2.5, 3.4 \leq x \leq 0\}$. The boundaries of the arterial lumen are described in the following way: $\partial\Omega_f = \Gamma_{fw} \cup \Gamma_f^{in} \cup \Gamma_f^{out}$, such that: $\Gamma_f^{in} = \{(x, y) : x = 0, 1.5 \leq y \leq 2.5\}$ and $\Gamma_f^{out} = \{(x, y) : x = 9.6, 0.5 \leq y \leq 1.5\} \cup \{(x, y) : x = 9.6, 3.5 \leq y \leq 4.5\}$. On the other hand, the boundaries of the wall domain are considered as: $\partial\Omega_w = \Gamma_{fw} \cup \Gamma_w \cup \Gamma_w^{in} \cup \Gamma_w^{out}$, such that: $\Gamma_w = \{(x, y) : y = 1.2, 0 \leq x \leq 3.4\} \cup \{(x, y) : y = -1/6.2x + 10.84/6.2, 3.4 \leq x \leq 9.6\} \cup \{(x, y) : y = -1/6.2x + 5.28/6.2, 9.6 \leq x \leq 3.4\} \cup \{(x, y) : y = 2.8, 3.4 \leq x \leq 0\}$, $\Gamma_w^{in} = \{(x, y) : y = 0, 1.5 \leq x \leq 1.2\} \cup \{(x, y) : y = 0, 2.8 \leq x \leq 2.5\}$ and $\Gamma_w^{out} = \{(x, y) : x = 9.6, 0.2 \leq y \leq 0.5\} \cup \{(x, y) : x = 9.6, 1.5 \leq y \leq 1.8\} \cup \{(x, y) : x = 9.6, 3.2 \leq y \leq 3.5\}$.

The current numerical test is performed by imposing the following boundary conditions. In the upstream of lumen Γ_f^{in} , we utilize parabolic profile by considering $u_x = 32.0(y - 1.5)(2.5 - y) \text{cm s}^{-1}$ and $u_y = 0$. On the interface Γ_{fw} , we assume no-slip boundary condition $\mathbf{u} = 0$ for the velocity vector field. Constant inflow condition $C_f = 1.0 \text{g cm}^{-3}$ and $C_w = 0.5 \text{g cm}^{-3}$ is considered for the solute concentration of the blood in the lumen and the arterial wall Γ_f^{in} and Γ_w^{in} , respectively. Homogeneous Neumann boundary condition $(-\nu \nabla \mathbf{u} + PI) \cdot n_f = 0$ and $\mu_f \nabla C_f \cdot n_f = 0$ are considered on Γ_f^{out} and Γ_w^{out} for the free out flow. On the interface between the lumen and wall Γ_{fw} , we utilized two interface conditions (9) and (10). We choose the parameters value in the following manner: the blood viscosity $\nu = 0.5 \text{cm}^2 \text{s}^{-1}$, the diffusivity in the lumen and wall $\mu_f = \mu_w = 0.5 \text{cm}^2 \text{s}^{-1}$, permeability $\zeta = 1.0 \text{cm s}^{-1}$. The final time, the time step size and the mesh size are considered as $T = 5.0 \text{s}$, $\Delta t = 0.001 \text{s}$ and $h_{max} = 0.1 \text{cm}$, respectively. Figures 3 and 4 present the velocity vector field, concentration of solute and the pressure contours without arteriosclerosis in the bifurcated artery for backward-Euler scheme (*BES*) and *BDF2*, respectively. As expected, the velocity profile, concentration of blood molecules, and pressure field appear regular and reasonably for the healthy cases. Obviously, one can observe the higher value of velocity in the upstream side of the artery, which leads to penetrating a large amount of solute to the arterial wall. On the other hand, the velocity in the downstream side of the artery gradually decreases, due to the bifurcation of the artery, which disturbs the uniform blood flowing, as a consequence, low concentration in the downstream side of the artery.

The impact of the gradual increases of the narrow size of the atherosclerosis on the blood flow in the bifurcated artery is illustrated in Figures 5 and 6, respectively. The flow speed, solute concentration, and pressure contour shows that the development of the atherosclerosis has a significant influence on the regular blood circulation. Hence, the bigger the stenosis, the obstacle is higher for the blood flow in the bifurcated artery.

In Figure 7, we present the efficiency and long-time stability of the *BDF2* scheme by illustrating the velocity profile for the final time $T = 1.0$ and $T = 10.0$, respectively. As expected, both figures appear in a similar pattern, which shows the long-time efficiency of the proposed method. On the other hand, Figure 8 presents the long-time behavior and stability of energy $\| \mathbf{u}_h \|_{L^2(\Omega_f)}^2 + \| C_{fh} \|_{L^2(\Omega_f)}^2 + \| C_{wh} \|_{L^2(\Omega_w)}^2$ at time-step level with different mesh-size $h_{max} = 0.1, 0.075, 0.05$, and 0.025 , respectively for the *BES* and *BDF2* schemes. The numerical results show that the varying mesh sizes do not affect the stability of the presented scheme.

6.3. The double stenoses artery in the case of physiological interest. The cardiovascular and the arterial disease illustrated that many stenoses might develop in the artery, which leads to irregular blood flow, as discussed in the previous experiment for the single stenosis. Thus the geometry of the artery has an important effect on the blood flow [55]. The main objective of this experiment is to investigate the magnitudes, streamlines, pressure field due to the presence of double stenoses. Moreover, we demonstrate the effect of the shear stress on the solute flux through the interfacial wall.

To perform the current simulation, we consider the double stenosis artery, which is shown in Figure 9. The interface between the lumen Ω_f and the wall Ω_w is assumed as $\Gamma_{fw} = \{(x, y) : y = 0, 0 \leq x \leq 3\} \cup \{(x, y) : y = 0.125(1 + \cos(2\pi x - 7\pi)), 3 \leq x \leq 4\} \cup \{(x, y) : y = 0, 4 \leq x \leq 8\} \cup \{(x, y) : y = 0.125(1 + \cos(2\pi x - 17\pi)), 8 \leq x \leq 9\} \cup \{(x, y) : y = 0, 9 \leq x \leq 12\}$. The blood solute distribution

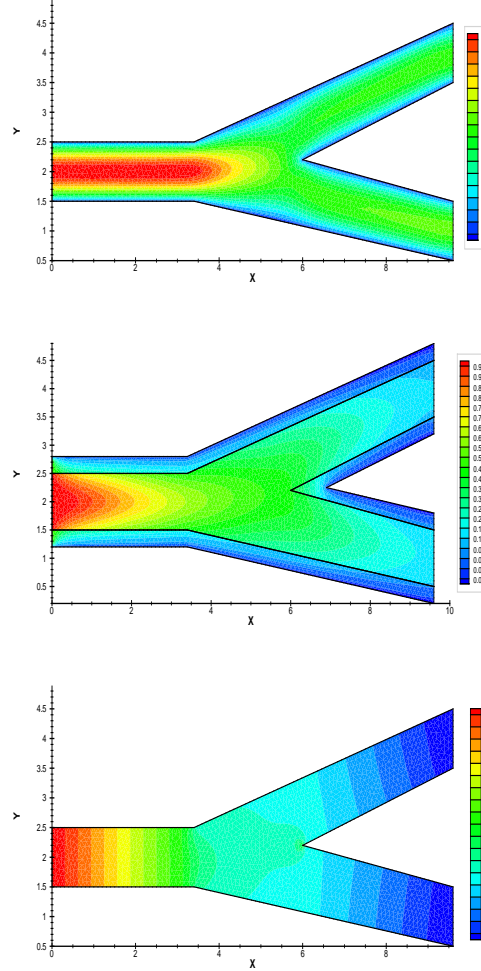


FIGURE 3. The bifurcated artery for the backward-Euler scheme (BES). Left: velocity profile. Right: concentration of solute. Down: pressure contour.

from the lumen to the arterial wall through the permeable endothelial layer Γ_{fw} is described by the two interface conditions (9) and (10).

In the upstream of the lumen Γ_f^{in} , we consider the parabolic profile $u_x = 15(1 - ((y - 0.5)/0.5)^2)$, $u_y = 0$ and the solute concentration $C_f = 1.0 \text{ g cm}^{-3}$. The homogeneous Neumann boundary condition $(-\nu \nabla \mathbf{u} + pI) \cdot n_f = 0$ and $\mu_f \nabla C_f \cdot n_f = 0$ are imposed in the downstream of the lumen Γ_f^{out} . On the other hand, no-slip boundary condition $\mathbf{u} = 0$ is imposed on $\Gamma_{fw} \cup \Gamma_f$. Moreover, we assume $C_w = 0.5 \text{ g cm}^{-3}$ on the boundary $\Gamma_w^{in} \cup \Gamma_w$ and $\mu_w \nabla C_w \cdot n_w = 0$ on the wall downstream Γ_w^{out} .

The parameters value of this numerical experiment are considered in the following way: the blood viscosity is $\nu = 0.033 \text{ cm}^2 \text{s}^{-1}$ and $\mu_f = \mu_w = 5.10^{-5} \text{ cm}^2 \text{s}^{-1}$ are the lumen and the wall diffusivity. The wall permeability ζ is given as a function of the shear stress $\sigma(u)$, $\zeta = K_1 + K_2 |\sigma(u)|$, such that $K_1 = 3.11 \cdot 10^{-3} \text{ cm}^{-1} \text{s}^{-1}$

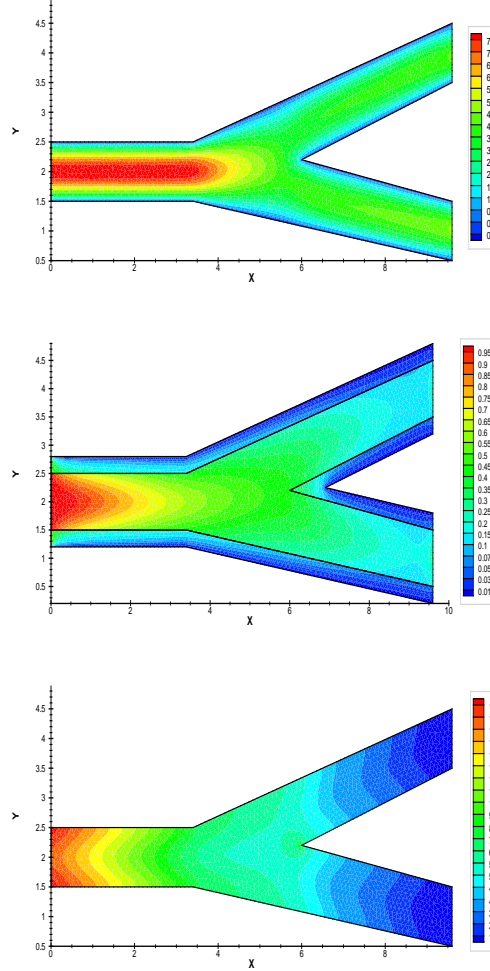


FIGURE 4. The bifurcated artery for *BDF2*. Left: velocity profile. Right: concentration. Down: pressure contour.

and $K_2 = 1.57 \cdot 10^{-4} \text{ cm}^3 \text{ dyn}^{-1} \text{ s}^{-1}$. The final time, the time step size and the mesh size are considered as $T = 1.0 \text{ s}$, $\Delta t = 0.0001 \text{ s}$, and $h = 1/50 \text{ cm}$, respectively.

Figures 11 and 12 show the concentration in the wall boundary, the permeability, and the shear stress on the wall. The highest value of the concentration in the lumen and the wall is located in the most constriction part of both stenoses.

The up plot of Figure 10 demonstrates the pressure in the double stenoses artery. One can see in the upstream side of the first stenosis, the pressure gradually decreases and get a lower value in the most constriction part of the artery. The pressure contour recovers but does not attain the higher values, thus again the lowest value in the second stenosis part of the artery. The middle plot of Figure 10 shows the velocity contours in a double stenosed artery, which illustrate that a higher magnitude of velocity is developed inside the constriction of the first stenosis, and slightly lower in the downstream part. On the other hand, the flow again developed and

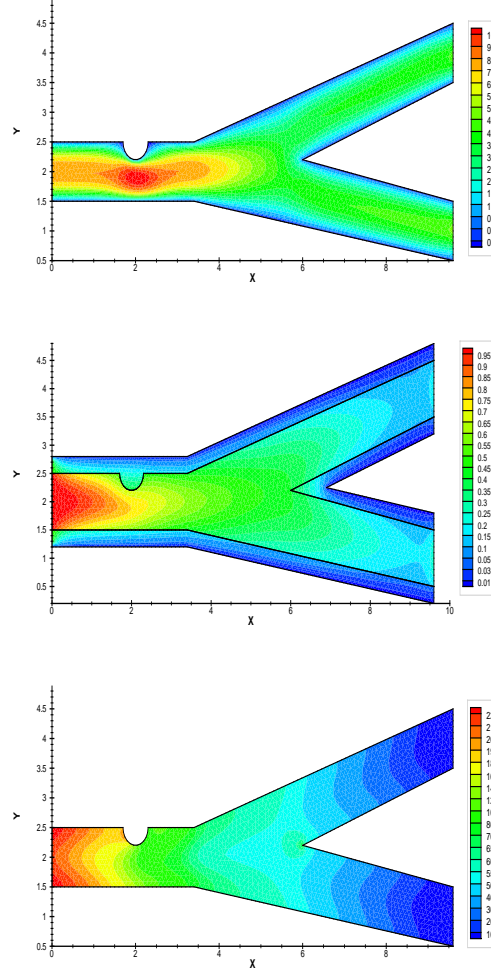


FIGURE 5. The bifurcated artery for *BDF2* with smaller atherosclerosis. Left: velocity profile. Right: concentration of solute. Down: pressure contour.

getting the highest value in the constriction of the second stenosis and gradually decreased in the downstream location. As expected, due to the stenosis presence, the streamlines are disturbed, which leads to a lack of the blood flow to another part of the artery. Thus recirculation zones appear in the downstream side of the first and the second stenosis, which is illustrated in the down plot of Figure 10.

6.4. Abdominal aortic aneurysm. One of the common cardiovascular diseases that occur in the abdominal aortic artery is the aneurysm, where the artery getting dilate at the weak area in the arterial wall. In this example, we investigate the velocity contours, streamlines, pressure field, and the wall shear stress through an aneurysmatic artery to understand the relation between the aneurysm development and the hemodynamic factors, such as blood pressure and the wall shear stress. In

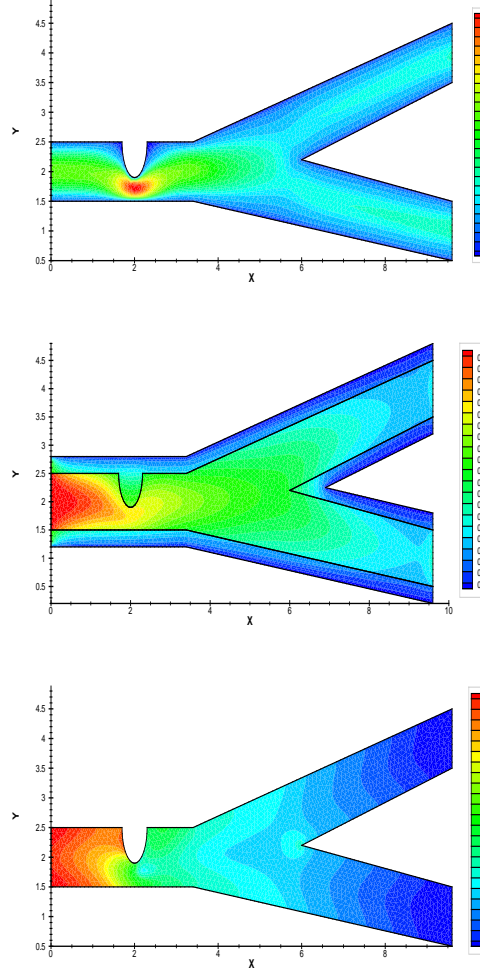


FIGURE 6. The bifurcated artery for *BDF2* with larger atherosclerosis. Left: velocity profile. Right: concentration of solute. Down: pressure contour.

addition, we study the development of the aneurysm by increasing the dilation of the diseased distinct [14].

The geometrical description of the aneurysmatic artery is shown in Figure 13. The common interface Γ_{fw} between the lumen Ω_f and the wall Ω_w is considered as: $\Gamma_{fw} = \{(x, y) : y = 0, 0 \leq x \leq 4\} \cup \{(x, y) : y = -a(1 + \cos(2\pi x - 9\pi)), 4 \leq x \leq 5\} \cup \{(x, y) : y = 0, 5 \leq x \leq 10\}$ where the interface conditions (9) and (10) are satisfied. The parameters value and the boundary conditions are imposed same as the previous numerical experiment, subsection 6.3.

Figure 14, illustrates the impact of the different aneurysmatic artery on the contours and streamlines due to the loss of arterial wall integrity. As expected, the vortices begin to appear for gradual increases of the aneurysm. Moreover, it is noted

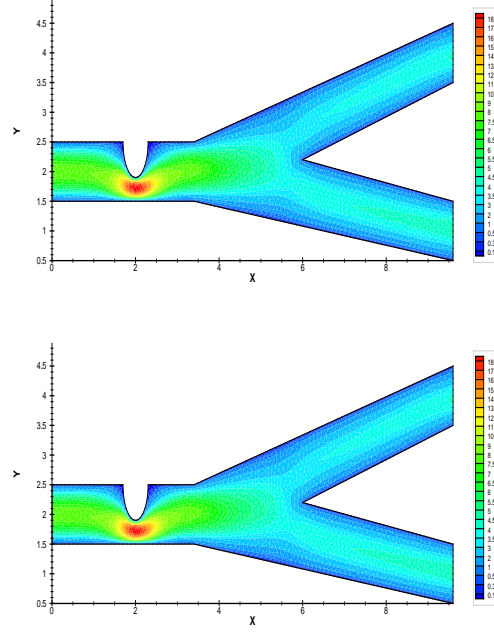


FIGURE 7. The bifurcated artery for *BDF2* with long-time stability for the different final time. Left: velocity profile for $T = 1.0$. Right: velocity profile for $T = 10.0$.

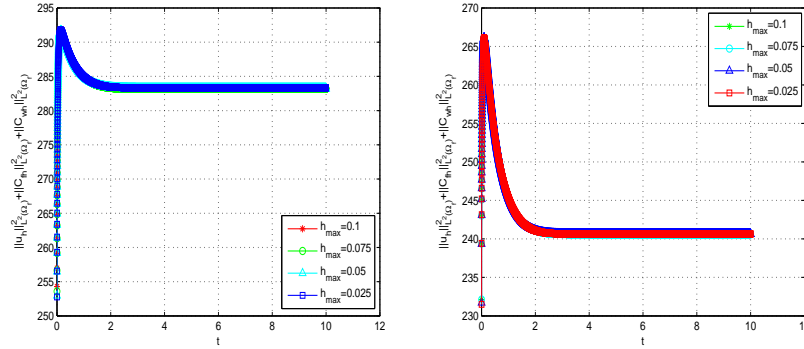


FIGURE 8. Energy vs Time on the time step points with different mesh sizes. Left: *BES*. Right: *BDF2*.

that the vortex size increases with the expansion of the balloon-shape aneurysm until it fills the entire aneurysm.

Figures 15 and 16 shows the concentration behavior and wall share stress on the interface Γ_{fw} . One can observe that the lower flow speed located in the dilation region of the artery, which leads to minimizing the values of the wall shear stress. As a result, a few concentrations located in the aneurysmatic area. On the other hand, the greater the size of the aneurysm produces the smaller shear stress on the

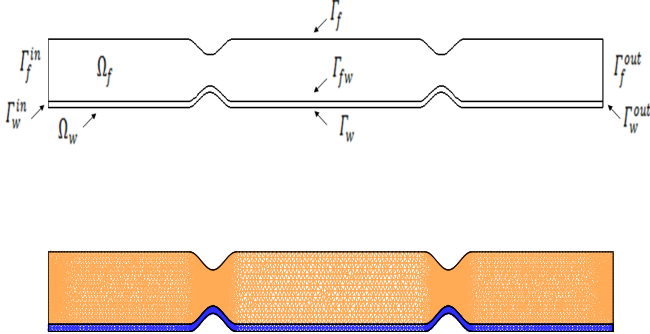


FIGURE 9. Up: a pictorial representation of the double stenoses artery. Down: illustration of the computational mesh.

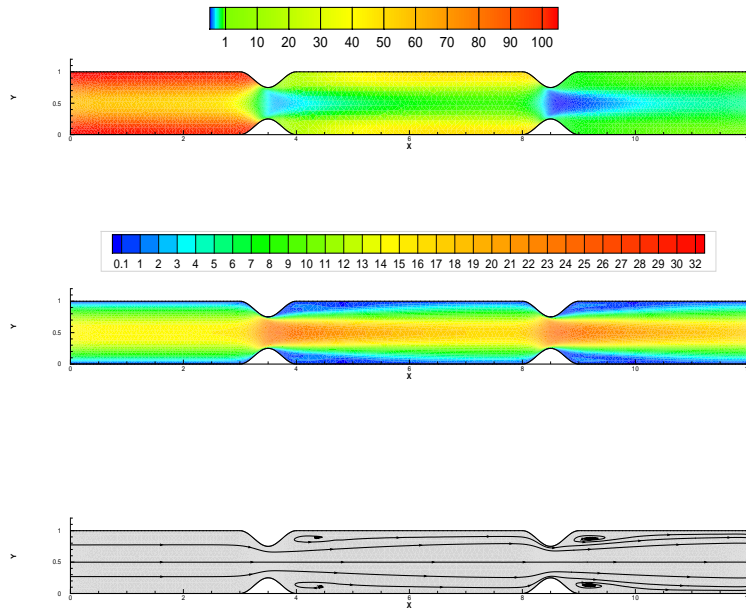


FIGURE 10. Up: the pressure contour for the double stenoses artery. Middle: the magnitudes and pressure contours for the velocity vector field. Down: the illustration of the streamlines for the velocity profile.

wall, which essentially leads to a lower concentration in the diseased region. The right plot of Figure 16 presents an important factor in hemodynamics which is the blood pressure distribution on the interface Γ_{fw} for different dilation size. One can observe that the pressure starts to decrease in the upstream part till it reaches the dilation of the artery where it starts again to develop until it reaches the highest values, while in the downstream part, the pressure gradually decreases.

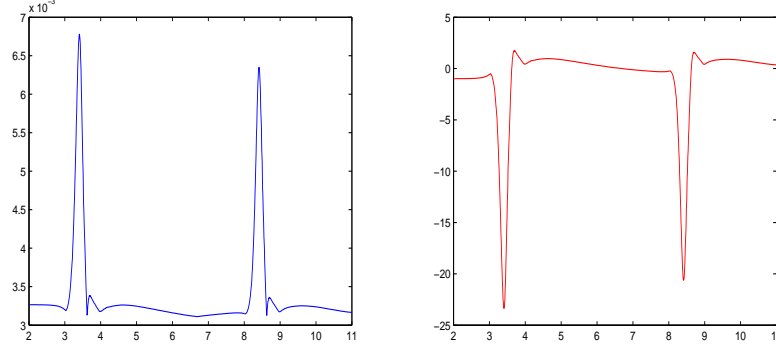


FIGURE 11. Left: arterial wall permeability on the interface Γ_{fw} . Right: arterial shear stress Γ_{fw} .

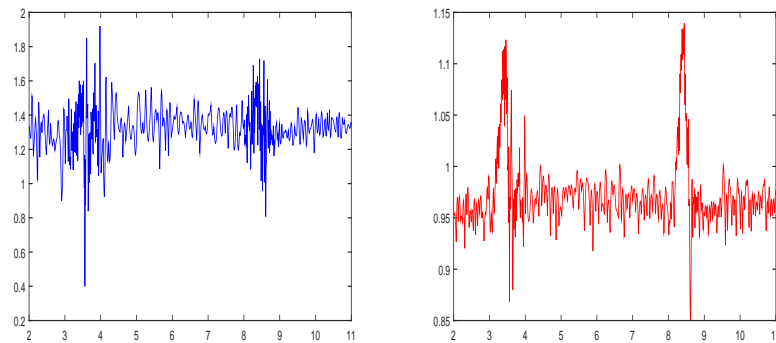


FIGURE 12. Solute concentration on the wall boundary. Left: lumenal concentration. Right: arterial wall concentration.

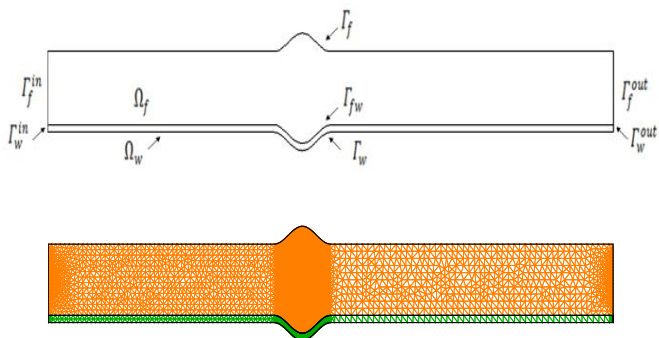


FIGURE 13. Up: the geometrical illustration of the abdominal aortic aneurysm. Down: representation of the computational mesh.

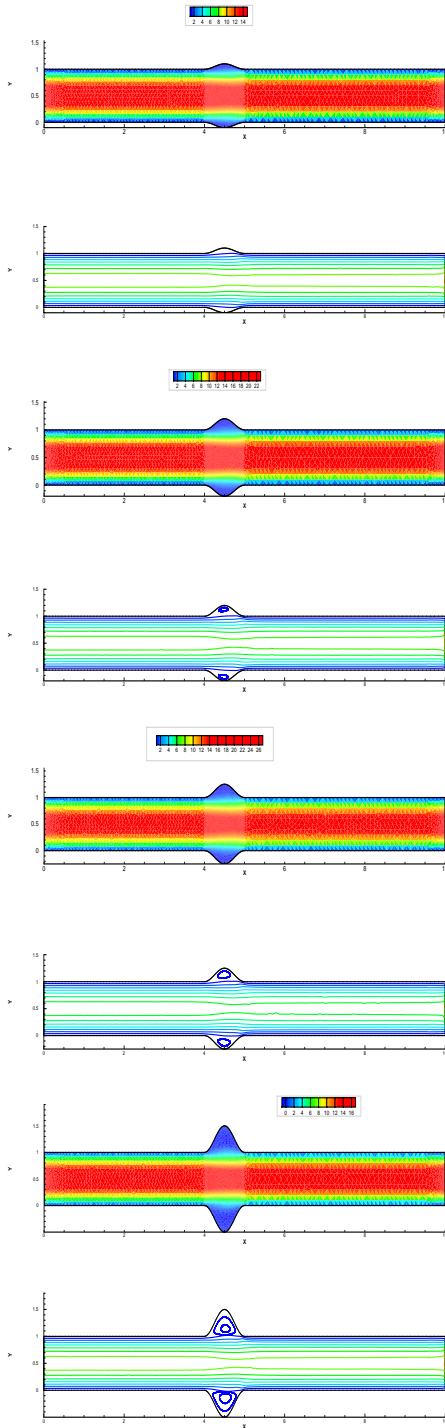


FIGURE 14. Velocity contours and streamlines for different aneurysmatic artery size $\Gamma_{fw} = \{(x, y) : y = 0, 0 \leq x \leq 4\} \cup \{(x, y) : y = -a(1 + \cos(2\pi x - 9\pi))\}$. Up: $a = 0.05$. Up-next: $a = 0.1$. Down-previous: $a = 0.125$. Down: $a = 0.25$.

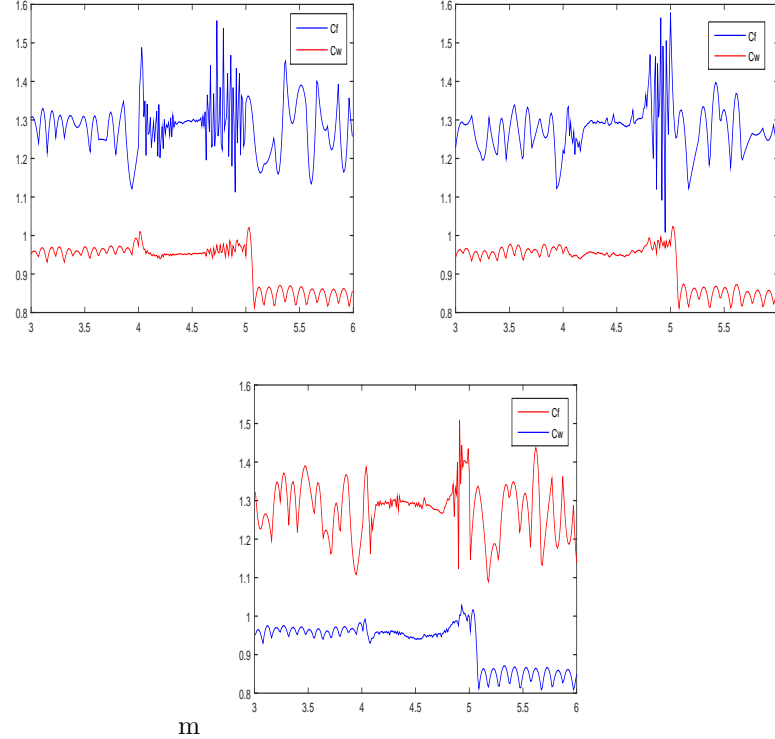


FIGURE 15. Solute concentration on the interface Γ_{fw} for different aneurysmatic artery size. Left: $a=0.05$. Middle: $a=0.1$. Right: $a=0.25$.

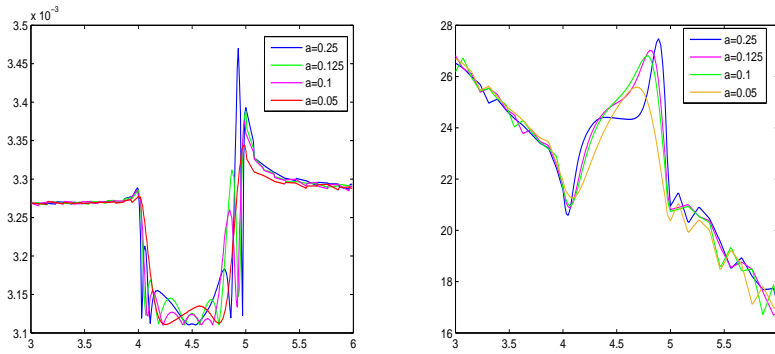


FIGURE 16. Left: wall shear stress distribution. Right: pressure distribution.

7. Conclusion

In this contribution, we investigate a sophisticated blood solute dynamic model where the blood flow is governed by the unsteady Navier-Stokes equation, and the solute concentration is modeled by the convection-diffusion equation. On the other

hand, the solute dynamics in the wall region is described by the pure diffusion equation. We propose a *BDF2* time-stepping scheme based on the second-order backward differentiation formulas and the explicit treatment of the interface terms. Therefore, two decoupled problems can be solved subsequently at each time step, hence the scheme can be implemented efficiently by using the legacy code. We show that the proposed algorithm is unconditionally stable and long-time stable in the sense that the solutions remain uniformly bounded in time. Moreover, the uniform in a time-bound of the solution further leads to uniform in time error estimates. The accuracy and the efficiency of the proposed numerical method are demonstrated by considering four numerical experiments that show the complicated flow characteristics, magnitudes, pressure field, solute concentration, wall shear stress, and long-time accuracy on the pseudo-realistic geometrical setups for the physiological interests.

Acknowledgments

The author acknowledges the anonymous reviewer's contribution by thanking them for their valuable comments which have significantly improved the manuscript. Partially supported by NSFC (No.12471406) and Science and Technology Commission of Shanghai Municipality No. 22DZ2229014 and Natural Science Foundation of Guangdong Province of China (No.2024A1515010294), and The University Grants Commission Research Project Funding of Comilla University, Bangladesh.

References

- [1] Back, L., Radbill, J. and Crawford, D., Analysis of Oxygen Transport from Pulsatile, Viscous Blood Flow to Diseased Coronary Artery of Man, *J. Biomech.*, 10, 763-774, 1977.
- [2] Nielson, L. B., Transfer of Low-Density Lipoprotein into the Arterial Wall and Risk of Atherosclerosis, *Atherosclerosis*, 123, 1-15, 1996.
- [3] Giddens, D. P., Zarins, C. K. and Glagov, S., The Role of Fluid Mechanics in the Localization and Detection of Atherosclerosis, *J. Biomed. Eng.*, 115, 588-594, 1993.
- [4] Baish, J. W., Netti, P. A. and Jain, R. K., Transmural Coupling of Fluid Flow in Microcirculatory Network and Interstitium in Tumors, *Microvasc. Res.*, 53, 128-141, 1997.
- [5] Lei, X. X., Wu, W. Y., Wen, G. B. and Chen, J. G., Mass Transport in Solid Tumors (I) - Fluid Dynamics, *Comput. Math. Methods Mech. Engrg.*, 19, 1025-1032, 1998.
- [6] Goldstick, T. K. and Dobrin, P. B., Arterial Wall Oxygen Transport and Its Relationship to Atherogenesis, in *Handbook of Bioengineering*, R. Skalak and S. Chen, eds., McGraw-Hill, New York, 1987, Chap. 22.
- [7] Prosi, M., Zunino, P., Perktold, K. and Quarteroni, A., Mathematical and Numerical Models for Transfer of Low-Density Lipoproteins through the Arterial Walls: A New Methodology for the Model Set Up with Applications to the Study of Disturbed Luminal Flow, *J. Biomech.*, 38, 903-917, 2005.
- [8] Karner, G., Perktold, K., Zehentner, H. P. and Prosi, M., Mass Transport in Large Arteries and through the Arterial Wall, Intra and Extracorporeal Cardiovascular Fluid Dynamics, Vol. 2, Fluid-Structure Interaction, *Adv. Fluid Mech.* 23, P. Verdonck and K. Perktold, eds., WIT Press-Computational Mechanics, Southampton, Bellerica, MA, 209-247, 2000.
- [9] Tarbell, J., Lever, M. and Caro, C., The Effect of Varying Albumin Concentration and Hydrostatic Pressure on Hydraulic Conductivity of the Rabbit Common Carotid Artery, *Microvasc. Res.*, 35, 204-220, 1988.
- [10] Olgac, U., Kurtcuoglu, V. and Poulikakos, D., Computational Modeling of Coupled Blood-Wall Mass Transport of LDL: Effects of Local Wall Shear Stress, *Am. J. Physiol. Heart Circ. Physiol.*, 294, 909-919, 2008.
- [11] Caro, C. G., Fitzgerald, J. M. and Schroter, R. C., Atheroma and Wall Shear: Observation, Correlation and Proposal of a Shear Dependent Mass Transfer Mechanism of Atherogenesis, *Proc. Roy. Soc. Lond. B*, 177, 109-159, 1971.

- [12] Golledge, J. and Norman, P. E., Atherosclerosis and Abdominal Aortic Aneurysm: Cause, Response, or Common Risk Factors?, *Arterioscler. Thromb. Vasc. Biol.*, 30, 1075-1077, 2010.
- [13] Scotti, C. M., Jimenez, J., Muluk, S. C. and Finol, E. A., Wall Stress and Flow Dynamics in an Abdominal Aortic Aneurysm: Finite Element Analysis vs. Fluid-Structure Interaction, *J. Comput. Methods Biomed. Eng.*, 11, 301-322, 2008.
- [14] Elhanafy, A., Guaily, A. and Elsaied, A., Numerical Simulation of Oldroyd-B Fluid with Application to Hemodynamics, *Adv. Mech. Eng.*, 11, 1-7, 2019.
- [15] Yang, N. and Vafai, K., Modeling of Low-Density Lipoprotein (LDL) Transport in the Artery-Effects of Hypertension, *Int. J. Heat Mass Transf.*, 49, 850-867, 2006.
- [16] Rappitsch, G. and Perktold, K., Pulsatile Albumin Transport in Large Arteries: A Numerical Simulation Study, *J. Biomech. Eng.*, 118, 511-519, 1996.
- [17] Rappitsch, G., Perktold, K. and Pernkopf, E., Numerical Modeling of Shear-Dependent Mass Transfer in Large Arteries, *Int. J. Numer. Methods Fluids*, 25, 847-857, 1997.
- [18] Jo, H., Dull, R. O., Hollis, T. M. and Tarbell, J. M., Endothelial Albumin Permeability Is Shear Dependent, Time Dependent and Reversible, *Am. J. Physiol.*, 260 1992-1996, 1991.
- [19] Wada, S. and Karino, T., Theoretical Prediction of Low-Density Lipoproteins Concentration at the Luminal Surface of an Artery with a Multiple Bend, *J. Biomed. Eng. Soc.*, 30, 778-791, 2002.
- [20] Karner, G. and Perktold, K., Numerical Modeling of Mass Transport in the Arterial Wall, in Proceedings of the 1999 Bioengineering Conference, BED, V.K. Goal, R.L. Spilker, G. A. Ateshian, and L. J. Solawsky, eds., ASME, New York, 42, 739-740, 1999.
- [21] Ethier, C. R. and Moore, J. A., Oxygen Mass Transfer Calculations in Large Arteries, ASME J. Biomech. Eng., 119, 469-475, 1997.
- [22] Quarteroni, A., Veneziani, A. and Zunino, P., Mathematical and Numerical Modeling of Solute Dynamics in Blood Flow and Arterial Walls, *SIAM J. Numer. Anal.*, 39, 1488-1511, 2001.
- [23] Quarteroni, A. and Valli, A., A Domain Decomposition Methods for Partial Differential Equations, Oxford University Press, Oxford, 1999.
- [24] Khakpour, M. and Vafai, K., Critical Assessment of Arterial Transport Models, *Int. J. Heat Mass Transf.*, 51, 807-822, 2008.
- [25] Mahbub, M. A. A., He, X., Nasu, N. J., Qiu, C. and Zheng, H., Coupled and Decoupled Stabilized Mixed Finite Element Methods for Non-Stationary Dual-Porosity-Stokes Fluid Flow Model, *Int. J. Numer. Methods Eng.*, 120, 803-830, 2019.
- [26] Mahbub, M. A. A., Shi, F., Nasu, N. J., Wang, Y. and Zheng, H., Mixed Stabilized Finite Element Method for the Stationary Stokes-Dual-Permeability Fluid Flow Model, *Comput. Methods Appl. Mech. Engrg.*, 358 (2020), 112616.
- [27] Mu, M. and Zhu, X., Decoupled Schemes for a Non-Stationary Mixed Stokes-Darcy Model, *Math. Comput.*, 270, 707-731, 2010.
- [28] Shan, L. and Zheng, H., Partitioned Time Stepping Method for Fully Evolutionary Stokes-Darcy Flow with Beavers-Joseph Interface Conditions, *SIAM J. Numer. Anal.*, 51, 813-839, 2013.
- [29] Zhang, J., Rui, H. and Cao, Y., A Partitioned Method with Different Time Steps for Coupled Stokes and Darcy Flows with Transport, *Int. J. Numer. Anal. Model.*, 16, 463-498, 2019.
- [30] Shan, L., Zheng, H. and Layton, W., A Decoupling Method with Different Sub-Domain Time Steps for the Nonstationary Stokes-Darcy Model, *Numer. Methods Partial Differential Equation*, 29, 549-583, 2013.
- [31] Layton, W., Tran, H. and Xiong, X., Stability of Four Methods for Splitting the Evolutionary Stokes-Darcy Problem into Stokes and Darcy Subproblems, *J. Comput. Appl. Math.*, 236 3198-3217, 2012.
- [32] Connors, J. M., An Ensemble-Based Conventional Turbulence Model for Fluid-Fluid Interaction, *Int. J. Numer. Anal. Model.*, 15, 492-519, 2018.
- [33] Layton, W., Tran, H. and Trenchea, C., Analysis of Long Time Stability and Errors of Two Partitioned Methods for Uncoupling Evolutionary Groundwater-Surface Water Flows, *SIAM J. Numer. Anal.*, 51, 248-272, 2013.
- [34] Jiang, N., A Second-Order Ensemble Method Based on a Blended Backward Differentiation Formula Time Stepping Scheme for Time-Dependent Navier-Stokes, *Numer. Methods Partial Differential Equations*, 33 (2016), 34-61.
- [35] Heister, T., Olshanskii, M. A. and Rebholz, L. G., Unconditional Long-Time Stability of a Velocity-Vorticity Method for the 2D Navier-Stokes Equations, *Numer. Math.*, 135, 143-167, 2016.

- [36] Hou, T. Y. and Wetton, B. T. R., Second-Order Convergence of a Projection Scheme for the Incompressible Navier-Stokes Equations with Boundaries, *SIAM J. Numer. Anal.*, 30, 609-629, 1993.
- [37] Layton, W. and Trenchea, C., Stability of the IMEX Methods, CNLF and BDF2-AB2 for Uncoupling Systems of Evolution Equations, *Appl. Numer. Math.*, 62, 112-120, 2012.
- [38] Chen, W. B., Gunzburger, M., Sun, D. and Wang, X. M., Efficient and Long-Time Accurate Second-Order Methods for Stokes-Darcy System, *SIAM J. Numer. Anal.*, 51, 2563-2584, 2013.
- [39] Chen, W. B., Gunzburger, M., Sun, D. and Wang, X. M., Efficient and Long-Time Accurate Third-Order Methods for Stokes-Darcy System, *Numer. Math.*, 134, 857-879, 2015.
- [40] Li, Y., Hou, Y. and Rong, Y., A Second-Order Artificial Compression Method for the Evolutionary Stokes-Darcy System, *Math. Method Appl. Sci.*, 41, 2178-2208, 2018.
- [41] Li, Y. and Hou, Y., A Second-Order Partitioned Method with Different Subdomain Time Steps for the Evolutionary Stokes-Darcy System, *Math. Method Appl. Sci.*, 41, 2178-2208, 2016.
- [42] Heister, T., Mohebujjaman, M. and Rebholz, L. G., Decoupled, Unconditionally Stable, Higher Order Discretizations for MHD Flow Simulation, *J. Sci. Comput.*, 71, 21-43, 2017.
- [43] Akbas, M., Kaya, S. and Rebholz, L. G., On the Stability at All Times of Linearly Extrapolated BDF2 Time Stepping for Multiphysics Incompressible Flow Problems, *Numer. Methods Partial Differential Equations*, 33, 999-1017, 2016.
- [44] Ravindran, S. S., Analysis of Second-Order Decoupled Time-Stepping Scheme for Transient Viscoelastic Flow, *Int. J. Numer. Anal. Model.*, 17, 87-109, 2020.
- [45] Adams, R. A., Sobolev Spaces, World Book Inc, 2009.
- [46] Wang, Y., Mahbub, M. A. A. and Zheng, H., Partitioned Schemes for the Blood Solute Dynamics Model by the Variational Multiscale Method, *Appl. Numer. Math.*, 198, 318-345, 2024.
- [47] Atrout, S., Mahbub, M. A. A. and Zheng, H., Decoupled Modified Characteristics Variational Multiscale Method for Solving the Blood Solute Dynamics Model, *Math. Comput. Simul.*, 211, 23-56, 2023.
- [48] Zhang, Y., Hou, Y. and Zhao, J., Error Analysis of a Fully Discrete Finite Element Variational Multiscale Method for the Natural Convection Problem, *Comput. Math. Appl.*, 68, 543-567, 2014.
- [49] Layton, W., Introduction to the Numerical Analysis of Incompressible Viscous Flows, Society for Industrial and Applied Mathematics, 2008.
- [50] Hairer, E. and Wanner, G., Solving Ordinary Differential Equations II: Stiff and Differential Algebraic Problems, 2nd Ed., Springer-Verlag, Berlin, 2002.
- [51] Ku, D. N., Giddens, D. P., Zarins, C. K. and Glagov, S., Pulsatile Flow and Atherosclerosis in the Human Carotid BifurcationPositive Correlation between Plaque Location and Low and Oscillating Shear Stress, *Arteriosclerosis*, 5, 293-302, 1985.
- [52] Lei, M., Kleinstreuer, C. and Truskey, G. A., A Focal Stress-Dependent Mass Transfer Mechanism for Atherogenesis in Branching Arteries, *Med. Eng. Phys.*, 18, 326-332, 1996.
- [53] Li, J., Jing, F., Chen, Z. and Lin, X., A Priori and A Posteriori Estimates of Stabilized Mixed Finite Volume Methods for the Incompressible Flow Arising in Arteriosclerosis, *J. Comput. Appl. Math.*, 363, 35-52, 2020.
- [54] Silva, T., Sequeira, A., Santos, R. F. and Tiago, J., Mathematical Modeling of Atherosclerotic Plaque Formation Coupled with a Non-Newtonian Model of Blood Flow, *Conference Papers in Mathematics*, ID 405914, 2013.
- [55] Rabby, M. G., Shupti, S. P. and Molla, M. M., Pulsatile Non-Newtonian Laminar Blood Flows through Arterial Double Stenoses, *J. Fluids*, 1-13, 2014.
- [56] Temam, R., Navier-Stokes Equations, Theory and Numerical Analysis, Sole Distributors for the U.S.A. and Canada, Elsevier North-Holland, 1984.

School of Mathematical Sciences and Shanghai Key Laboratory of Pure Mathematics and Mathematical Practice, East China Normal University, Shanghai, P. R. China.

E-mail: atroutsabah@hotmail.com

Department of Mathematics, Comilla University, Cumilla 3506, Bangladesh.

E-mail: dipmahbub13@cou.ac.bd

School of Mathematical Sciences, East China Normal University, Shanghai, P. R. China.

E-mail: 52275500026@stu.ecnu.edu.cn

School of Mathematical Sciences, Ministry of Education Key Laboratory of Mathematics and Engineering Applications, Shanghai Key Laboratory of PMMP, East China Normal University, Shanghai.

E-mail: hbzheng@math.ecnu.edu.cn